STL-based analysis of TRAIL-induced apoptosis challenges the notion of type I/type II cell line classification

Szymon Stoma, Alexandre Donzé, François Bertaux, Oded Maler, Grégory Batt

STL-based analysis of TRAIL-induced apoptosis challenges the notion of type I/type II cell line classification

Szymon Stoma, Alexandre Donzé, François Bertaux, Oded Maler, Gregory Batt

RESEARCH REPORT

N° 8121

30/10/2012

Project-Team CONTRAINTES

ISSN 0249-6399

STL-based analysis of TRAIL-induced apoptosis challenges the notion of type I/type II cell line classification

Szymon Stoma[1,#], Alexandre Donzé[2,#,$], François Bertaux[1], Oded Maler[2] and Gregory Batt[1]

[1] INRIA Paris-Rocquencourt, 78153 Le Chesnay Cedex, France
[2] VERIMAG, CNRS and the University of Grenoble, Gières, France

Research Report N° 8121 — 30/10/2012 —35 pages.

Abstract: Extrinsic apoptosis is a programmed cell death triggered by external ligands, such as the TNF-related apoptosis inducing ligand (TRAIL). Depending on the cell line, the specific molecular mechanisms leading to cell death may significantly differ. Precise characterization of these differences is crucial for understanding and exploiting extrinsic apoptosis. Cells show distinct behaviors on several aspects of apoptosis, including *(i)* the relative order of caspases activation, *(ii)* the necessity of Mitochondria Outer Membrane Permeabilization (MOMP) for effector caspase activation, and *(iii)* the survival of cell lines overexpressing Bcl2, leading to classification of cell lines into two groups (type I and type II).

In this work we challenge this type I/II cell line classification. We encode the three aforementioned distinguishing behaviors in a formal language, called signal temporal logic (STL), and use it to extensively test the validity of a previously-proposed model of TRAIL-induced apoptosis with respect to experimental observations made on different cell lines. Then, STL-guided parameter search is used to solve the few inconsistencies found between model and data. We show that these three criteria do not define consistent cell line classifications in type I or type II, and suggest mutants that are predicted to exhibit ambivalent behaviors. In particular, this finding sheds light on the role of a feedback loop between caspases, and reconciliates two apparently-conflicting views regarding the importance of either upstream or downstream processes for cell type determination. More generally, our work suggests that rather than being considered as defining criteria for cell type classification, these three distinguishing behaviors should be merely considered as type I or II features.

On the methodological point of view, this work illustrates the biological relevance of STL-diagrams, STL population data, and STL-guided parameter search. Such tools are well adapted to the ever-increasing availability of heterogeneous knowledge on complex signal transduction pathways.

[#] Denotes equal contributions
[$] Present address: EECS Department, University of California Berkeley, Berkeley, USA

RESEARCH CENTRE
ROCQUENCOURT

Domaine de Voluceau
Rocquencourt BP 105
78153 Le Chesnay Cedex France

Une étude de l'apoptose induite par TRAIL basée sur STL questionne la pertinence d'une classification des lignées cellulaires en types I ou II

Résumé: L'apoptose extrinsèque est un processus de mort cellulaire programmée qui est activé par la présence de ligands extracellulaires, tels que TRAIL (TNF-related apoptosis inducing ligand). Selon la lignée cellulaire, les mécanismes spécifiques qui mènent à la mort cellulaire diffèrent. La caractérisation de ces différences est essentielle pour comprendre et pouvoir exploiter à des fins thérapeutiques la réponse apoptotique des cellules. Plusieurs aspects de l'apoptose diffèrent d'une lignée cellulaire à l'autre dont notamment /(i)/ l'ordre relatif de l'activation des caspases, /(ii)/ la nécessité de la MOMP (mitochondria outer membrane permeabilization) pour l'activation des caspases effectrices, et /(iii)/ la survie des lignées cellulaires qui surexpriment Bcl2, ce qui a conduit à classifier les lignées cellulaires en deux groupes, dits type I et type II.

Dans ce travail, nous discutons cette classification en type I ou II. Nous encodons les trois comportements distinctifs mentionnés plus haut dans un langage formel, appelé STL (signal temporal logic), et testons la validité d'un modèle précédemment publié de l'apoptose induite par TRAIL par rapport à des observations expérimentales réalisées sur différentes lignées cellulaires. Puis, nous utilisons de la recherche de paramètres guidé par les propriétés de STL pour résoudre quelques incompatibilités détectées entre modèle et données. Nous montrons que ces trois critères différents ne définissent pas une classification cohérente des lignées cellulaires en type I ou II, et suggérons des mutants susceptibles de présenter des comportements ambivalents. En particulier, ces résultats soulignent l'importance d'une boucle de rétroaction entre caspases, et réconcilie deux visions apparemment contradictoires sur l'importance des processus amonts ou avals pour la détermination du type cellulaire. Plus généralement, notre travail suggère que plutôt que d'être considérés comme des critères de définition pour la classification des lignées cellulaire en deux types, ces comportement distinctifs devraient être simplement regardés comme des caractéristiques de type I ou II.

Du point de vue méthodologique, ce travail illustre la pertinence des diagrammes STL, des données de population STL, et de la recherché de paramètres guidés par des formules en STL. De tels outils sont bien adaptés à l'acquisition de plus en plus rapide de connaissances hétérogènes sur des voies de transduction du signal complexes.

Introduction

Apoptosis, a major form of programmed cell death, plays a crucial role in shaping organs during development and controls homeostasis and tissue integrity throughout life [1,2]. It can be triggered by *intrinsic* or *extrinsic* stimuli. Intrinsic apoptosis is triggered in case of cell damage (e.g. stress, UV radiation) or cell malfunction (e.g. oncogene activation). Extrinsic apoptosis is initiated by the presence of extracellular death ligands, such as Fas ligand (FasL), Tumor Necrosis Factor (TNF), or TRAIL [2]. Because the latter has a unique ability to trigger apoptosis in various cancer cell lines without significant toxicity toward normal cells, TRAIL-induced apoptosis has been the focus of extensive studies [1].

The effects of TRAIL application can be significantly different from one cell line to another [3–5]. The current understanding is that cell death results from the activation of one of two parallel pathways, leading to the classification of cell lines into two distinct cell types. In type I cells, effector caspases are directly activated by initiator caspases. Mitochondria outer membrane permeabilization (MOMP) is not required to generate lethal levels of caspase activity. In type II cells, the activation of initiator caspases triggers MOMP that in turn triggers effector caspases activation. MOMP is required for cell death. This necessity of mitochondrial pathway activation to undergo apoptosis is often referred as *type II phenotype*, in contrast to *type I phenotype* where MOMP pathway activation is rather a side effect than the cause of apoptosis.

Depending on the experimental approach employed, different distinct behaviors have been observed between type I and II cells. A first distinction between cells is the ability of the derived cell lines overexpressing Bcl2 (OE-Bcl2 cells) to survive following TRAIL treatments. Because Bcl2 overexpression is known to inhibit MOMP by sequestrating Bax, which oligomerization creates pores in the mitochondrial membrane, this criterion assesses the crucial role of MOMP for cell death. This experimental setup is very attractive because it provides a clear outcome. However, it is an *indirect* method, since the observations are not made on the original cell lines, but on their OE-Bcl2 mutants instead. A second distinction between cell lines concerns initiator and effector caspases activations. Using a combination of antibody labeling and Western blots or flow cytometry, caspase activities can be directly measured. In type I cells, the activations of initiator and effector caspases are rapid and relatively synchronous, whereas in type II cells, they are delayed and sequential [4,5]. Recently, the central role of MOMP has been addressed directly on non-derived cell lines using time lapse microscopy and fluorescent reporters [2,6,7]. Even if MOMP always eventually happens, it has been observed that some but not all cell lines show significant effector caspase activity before MOMP [5]. A third distinguishing criteria is therefore that MOMP is not always required for cell death. Therefore, in the literature, several experimental setups have been developed to investigate the relative importance of the two pathways in different cell lines and suggest cell line classifications. Their consistency has however not been thoroughly challenged.

In accordance with the specific focus of particular experimental setups, different explanations have been proposed for the origin of these two distinct behaviors. Scaffidi et al. (1998) and Barnhart et al. (2003) suggest that the initiator caspase activation capabilities are the main determinants of the type I/II phenotype of a cell line, whereas Eissing et al. (2004), Jost et al. (2009), and Aldridge et al. (2011) suggest that the latter is mainly controlled by the relative abundance of downstream proteins, most notably XIAP and caspase-3. Since published studies use different cell lines and experimental techniques, it is non-trivial to assess whether one of the two proposed mechanisms alone is enough to explain all observations, or whether both mechanisms are needed. Answering these questions is important since this would solve a long-standing open question.

Here we propose an approach to investigate these questions in a systematic manner using mathematical modeling. Many models of apoptosis, based on different mathematical formalisms, ranging from logical models to differential equation systems [10], have been proposed so far [2,5,9,11–24]. Our work builds upon and

extends the work of Aldridge and colleagues. In Aldridge et al. (2011), the authors developed an ordinary differential equation (ODE) model describing key biochemical steps in TRAIL-induced apoptosis: extrinsic apoptosis reaction model (EARM1.4). Importantly, the differences between various cell lines were simply reflected by differences in the initial concentrations of a dozen of key apoptotic proteins, measured by quantitative immunoblotting. Here, to systematically analyze the behavior of selected cell lines we introduce the notion of *property-induced phase diagrams*, that extend the DLE phase diagrams introduced by Aldridge and Haller (2006) and extensively used by Aldridge and colleagues (2011). In short, for every initial protein concentration, one predicts the behavior of the system and assesses whether this behavior satisfies the given property, or more generally, estimates the value of the property given the behavior. Then one can graphically represent the value of the property in the state space by so-called phase diagrams. The placement of the cell lines in the phase diagram, based on their initial protein concentrations, reveals whether the cell line satisfy the given property. In this study, we use a formal language, Signal Temporal Logic (STL), to encode the various observed cellular responses associated with type I/II phenotypes. In contrast, Aldridge and colleagues used direct finite-time Lyapunov exponents to define their diagrams. In short, the DLE is an abstract criterion that measures the influence of changes in initial protein concentrations on the future state of the system (i.e. divergence of trajectories). Because DLEs somehow captured fundamental distinguishing features of cell type I and II behaviors, the authors were able to use it successfully to identify important determinants of the type I and II phenotypes. Here, because we use a language that allows us to express various observations made on cell lines, we can investigate *in which respect are the cell lines different*. Indeed, different STL properties induce different phase diagrams that can be directly compared. In addition to offering an intuitive, yet flexible and precise way to formalize observations, STL also possess a quantitative interpretation of properties. A positive property value indicates a satisfied property, and the higher the value, the higher the level of satisfaction. A negative value indicates a falsified property, and the lower the value, the higher the level of violation. This facilitates the interpretation of phase diagrams (DLEs in contrast are always positive), and more importantly allows defining statistics across populations of cells (e.g. mean value, percentage of satisfaction).

We consider three properties probing in subtly different manners the role of MOMP for apoptosis and often associated with cell type classification: death/survival following apoptosis stimulation of the derived cell line overexpressing Bcl2 (Property 1), synchronous/sequential activation of initiator and effector caspases (Property 2), and effector caspase activation prior/posterior to MOMP (Property 3). We also consider three cell lines: SKW6.4 (human B lymphoma cells), HCT116 (human colon carcinoma cells), T47D (human breast carcinoma cells), and all the derived cell lines obtained by overexpressing Bcl2 (OE-Bcl2) and/or by knocking out XIAP (ΔXIAP) [5,26,27]. For each property we propose an STL encoding and compute the corresponding phase diagram. We then investigate its consistency with the expected (i.e. measured in experiments) behaviors of the different cell lines.

We found several inconsistencies between STL diagrams and actual observations. An important discrepancy concerns the ΔXIAP HCT116 cells and the property stating that effector caspases are activated prior to MOMP. Indeed, unlike EARM1.4 predictions, it has been observed that in a majority of cells MOMP precedes caspases-3 activation [5]. More generally, this result highlights that the ΔXIAP HCT116 cell line exhibits a peculiar behavior: it should be classified as type II based on Properties 1 and 2, and as type I based on Property 3. Discrepancies concern also T47D cells. However they are known to manifest mixed type behavior with respect to clonogenic assay [5], they cluster with type I cell lines by transcriptional profiling [26] and behave like type II cells with respect to cytochrome c localization after PARP cleavage [5]. The behavior of these cells is therefore particularly puzzling and it is not surprising that EARM1.4 fails to capture all their specificities.

To investigate whether it is possible to reconcile the EARM1.4 model with all observed properties on HCT116 and SKW6.4 cells, we searched for parameters such that all properties where having the desired value for all cell lines. Here again we took advantage of our STL framework since it allowed us to define in a natural manner a real-valued cost function that is minimal when all properties have their expected values (i.e. are consistent with experimental data). Then using state-of-the-art global optimization tools we have been able to find valid parameters, thus showing that the current set of reactions can account for all observations without the need to include additional biomolecular processes in the EARM1.4.

Having encoded experimental characterization of type I/II behaviors in STL made it also easy to investigate whether the origin of the differences in behaviors could be explained solely by differences in upstream protein concentrations, solely by differences in downstream protein concentrations, or only by a combination of the two. Our results suggest that modifying the concentration of upstream proteins within physiological range has a negligible effect on cellular responses. However, the detailed analysis of the interactions between upstream and downstream proteins showed that the effects of downstream protein concentration differences are fed back to upstream processes and are amplified via a positive feedback loop involving caspases 3, 6, and 8. This finding reconciliates the views expressed by Scaffidi et al. (1998) and Aldridge et al. (2011) about the origins of type I and II phenotypes. Finally, the comparison of the STL and DLE diagrams showed that the DLE criterion essentially captures the notion of survival or death in OE-Bcl2 cells: DLE and Property 1 diagrams are identical. This lead us to better understand why the fairly abstract DLE criterion induced biologically-relevant partitions in the work of Aldridge et al. (2011).

A last contribution is that we extended the functionalities of the Breach tool so that phase diagrams can be automatically computed given any differential equation model and STL property [28]. Therefore, the methodology presented here can be applied to other complex biomolecular networks.

The first three sections of the Results part deal with the detailed analysis of three different observed phenotypes associated with type I/II behavior, encoded in STL, and confronted with model predictions. In the last two sections, we study whether the EARM model can be reconciled with all the considered observations on all cell lines and search for the origins of cell type differences.

Results

Property 1: Type II cells survive if Bcl2 is over-expressed

Bcl2 over-expression is the standard experimental method for distinguishing type I and type II cells [4]. Type I cells overexpressing the anti-apoptotic protein Bcl2 die in the presence of death ligand but type II cells survive. Indeed, in type II cells the sequestration of Bax by high levels of Bcl2 prevents the formation of pores in the mitochondrial outer membrane (Figure 1).

Clonogenic survival of an OE-Bcl2 derived cell line reveals the need for MOMP to trigger cell death in this cell line. Here, we formally specify this property and use EARM1.4 to compute phase diagrams and evaluate the property value across cell populations. We then compare these data with the experimental findings as well as the DLE-based classification proposed in Aldridge et al. (2011). The property is encoded in a formal language named STL. STL was originally developed for monitoring physical systems, such as analog electrical circuits [35]. Since it allows specifying and checking the validity of properties in time-series data, it applies naturally to the analysis of biomolecular reaction networks [36].

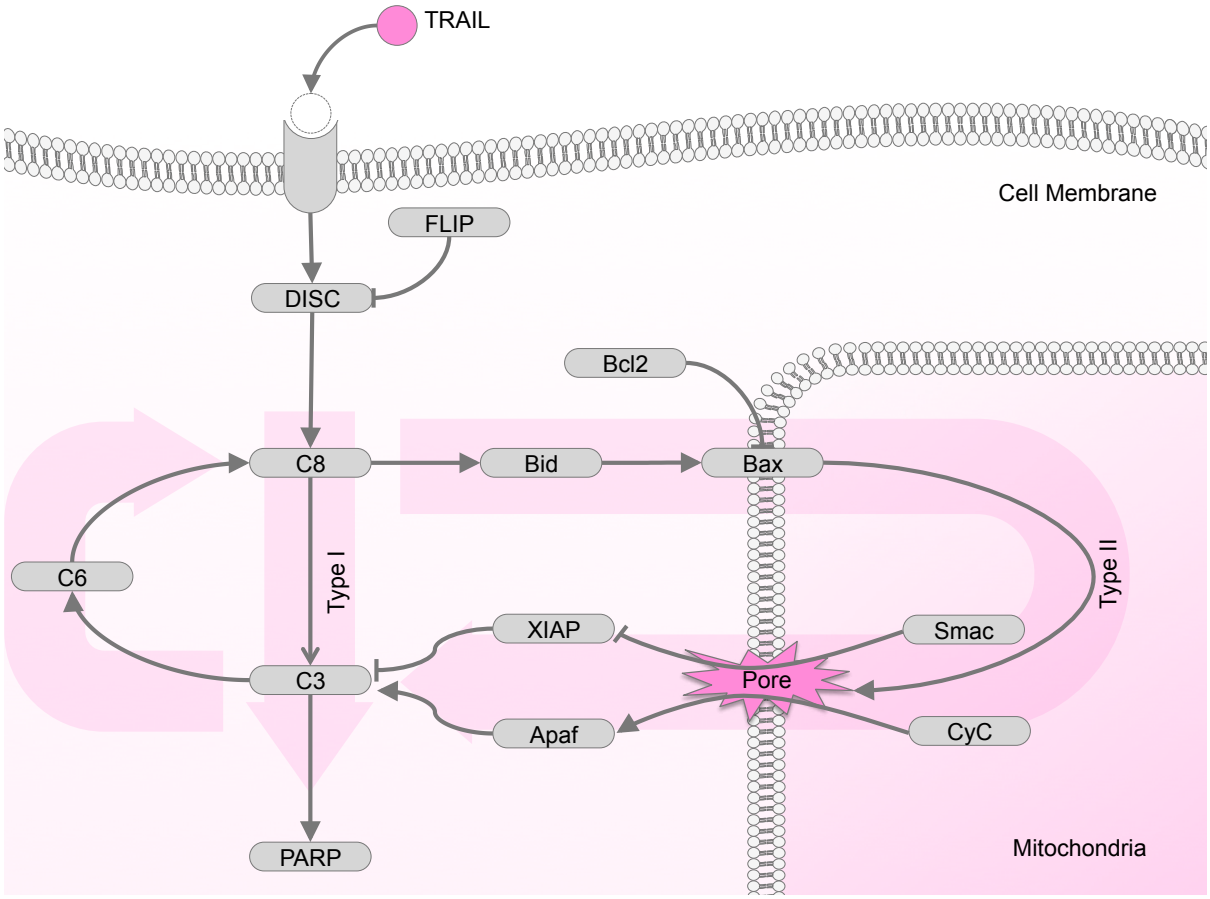

Figure 1. Simplified view on TRAIL-dependent apoptotic pathway. The activation of the membrane receptor by TRAIL binding promotes the assembly of the death-inducing signaling complexes (DISC), which recruit and activate initiator (pro-) caspases, including notably caspase-8 (C8) [29]. The recruitment of initiator caspases is modulated by FLIP. Once activated, initiator caspases cleave and activate effector caspases such as caspase-3 (C3). This effect is reinforced by a feedback loop involving caspase-6 (C6). Effector caspases cleave essential structural proteins, inhibitors of DNase, and DNA repair proteins (PARP), eventually leading to cell death. The cellular effect of effector caspase activation is regulated by factors such as the X-linked inhibitor of apoptosis protein (XIAP), which blocks the proteolytic activity of caspase-3 by binding tightly to its active site [30] and promotes its degradation via ubiquitination [31]. In addition to the direct activation of effector caspases, initiator caspases also activate Bid and Bax [32]. If not kept in check by inhibitors, most notably Bcl2, activated Bax directly contributes to the formation of pores in the mitochondria outer membrane, leading to MOMP [33]. Following MOMP, critical apoptosis regulators, such as Smac and cytochrome c (CyC), translocate into the cytoplasm. Smac binds to and inactivates XIAP, thus relieving the inhibition of effector caspases by XIAP [34]. Cytochrome c combines with Apaf-1 to form the apoptosome that in turn activates the initiator caspase-9 that activates effector caspases.

Effector caspases cleave essential structural proteins and inhibitors of DNase, leading to the digestion of chromosomal DNA and eventually to cell death. PARP is a substrate of these effector caspases and its cleavage is often regarded as a marker of commitment to death by cells [18,19,37]. Therefore, we consider here that a cell is dead if at least half of the PARP proteins are cleaved. In STL, this translates into: $alive := cPARP/PARP_{total} < 0.5$. Note that although the 50% threshold used here is somewhat arbitrary, we found that our conclusions are robust with respect to threshold changes in the range 10%-90% (see Figure S1). Because this property obviously depends on time, we may write $alive(t) := cPARP(t)/PARP_{total}(t) < 0.5$ to explicit this time dependence. Then the cell survival over the course of the experiment is simply expressed in STL as the cell is always alive: $Property1 := always(alive)$. Note that here, *always* is an STL keyword. Also, to mimic the clonogenic survival experiments made in Aldridge et al. (2011), we limited the scope of the *always* operator to the first 6 hours, denoted by $always_{[0\text{-}6h]}(alive)$. Many other properties on cell behaviors can be expressed similarly using this and other temporal operators, including *eventually* and *until*. These operators makes it

easier to go from an hypothesis on the mechanistic functioning of the system, expressed in natural language and taken from available biological knowledge, to a formal specification which can be computationally verified and tested *in silico* in a systematic computational framework (see Methods for details). Many other formal verification frameworks have been proposed and applied to systems or synthetic biology problems [38–45].

Given an ODE model, initial conditions and an STL property, one can automatically construct the phase diagram associated with two variables of interest. Since it has been shown that the ratio of XIAP to caspase-3 concentrations plays a key role for the determination of the apoptotic type [5], we first constructed diagrams associated with XIAP and caspase-3. The death/survival property is tested in derived cell lines where Bcl2 is overexpressed (OE-Bcl2 cells). That is why we used as initial conditions the nominal protein concentrations of HCT116 cells with a 10-fold increase of the Bcl2 concentration (see Methods). For many different values of initial concentrations of XIAP and caspase-3, spanning a range of protein concentrations actually found in different cell lines, we computed the cell behavior predicted by the model, and then assessed whether this behavior satisfied our property of interest, or more precisely, computed the value of the property associated with this behavior (see Methods and Figure 2). This resulted in the diagram represented in Figure 3. It should be noted that with the exception of XIAP and caspase-3 concentrations, all other initial protein concentrations were kept unchanged. To intuitively explain how the property values are computed, we represent in Figure 2 the details of the evaluation of Property 1 for the HCT116 and SKW6.4 cells (see also Methods). The presence of two distinct regions in the diagram, one where Property 1 is satisfied (positive values, green) corresponding to cell survival, typical of type II cells, and one where Property 1 is falsified (negative values, red) corresponding to cell death, typical of type I cells, suggests that the model correctly predicts the importance of the XIAP/caspase-3 ratio as a key factor to determine cell survival following TRAIL treatment. We then positioned cell lines in the diagram based on measured mean and standard deviation of protein concentrations (Methods and Aldridge et al. (2011)). In agreement with the observations (Figure 2B of Aldridge et al. (2011)) and the known type of these cell lines, the STL diagram predicts that OE-Bcl2 HCT116 cells do satisfy Property 1, but SKW6.4 cells do not. T47D cells are located close to separatrix and mostly satisfy Property 1. This is only in partial agreement with the fact that only half of T47D cells were found to survive (Figure 7C of Aldridge et al. (2011)). Interestingly, as noted in Aldridge et al. (2011), one can immediately see the consequences of mutations. For example, ΔXIAP cell lines are shifted to the leftmost part of the diagram (regions with low XIAP concentrations) and are thus predicted to violate Property 1. That is, all OE-Bcl2/ΔXIAP mutants of the HCT116, SKW6.4, and T47D cell lines are predicted to die. This is again in accordance with experimental observations for HCT116 cells (Figure 2B of Aldridge et al. (2011), data not available for SKW6.4, and T47D cells).

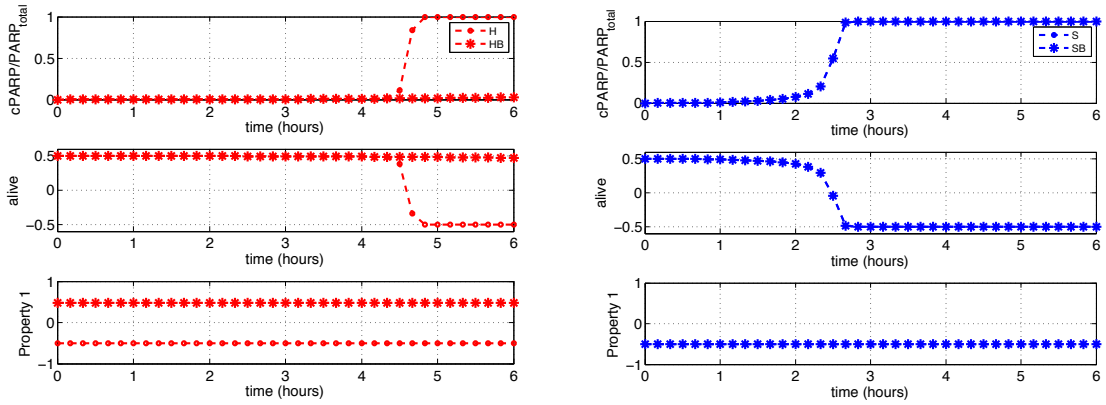

Figure 2: Evaluation of STL properties. Temporal evolution of the ratio $cPARP/PARP_{total}$, of the value of the property $alive$:= $cPARP/PARP_{total}<0.5$, and of $Property\ 1$:= $always_{[0\text{-}6h]}(\ cPARP/PARP_{total}< 0.5)$ for HCT116 and OE-Bcl2 HCT116 cells (left), and SKW6.4 and OE-Bcl2 SKW6.4 cells (right). When the concentration of cleaved PARP increases, the value of the $alive$ property gradually decreases

from a positive value ("true") to a negative value ("false"), and that the Property 1 simply captures whether at all times *alive* holds or not. More precisely, *Property 1* simply evaluates to the minimal value of *alive* at all times. The semantics of STL is described in details in [46].

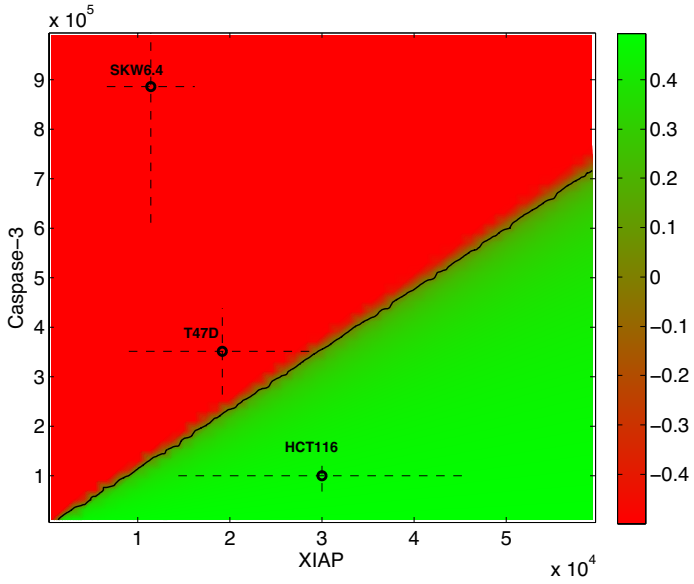

Figure 3. Property-1 phase diagram. Each point in the diagram represents a different initial concentration for XIAP and caspase-3 proteins, and its color represents the value of Property 1 ($p1 := always_{[0\text{-}6h]}(cPARP/PARP_{total} < 0.5)$). Green regions satisfy the property (positive values). Red regions do not (negative values). Cell lines can be positioned in this diagram, using crosses which center and size are determined by the mean and standard deviation of measured protein concentrations (Methods and [5]).

The phase diagrams computed with respect to Property 1 or to the DLE value used by Aldridge and colleagues present striking similarities: two regions delimited by a separatrix present at the same place (Figure S2A-B). The same holds if Property 1 or the DLE are evaluated at different times (Figure S2C-D). This reveals that the DLE criterion, like our Property 1, captures precisely the existence of two different possible outcomes: survival or death. High values for the DLE at time t are obtained for initial protein concentrations leading to the death of the cell at a time close to t. However, in full generality the DLE simply measures the influence of small changes in initial protein concentrations on the future state of the system. In fact, this comes from the *snap-action* aspect of apoptotic cell death, captured by the EARM model: cell death is immediately preceded by a sudden activation of effector caspases (all-or-none behavior) [18]. Due to snap-action, small changes in initial protein concentrations will result in dramatic differences in protein concentrations at the time of death. The successful classification of cells provided by Aldridge and colleagues *implicitly* relies on this aspect of apoptosis. Using the approach we propose here, the property of interest is *explicitly* stated and the interpretation of the resulting diagrams is not ambiguous. Moreover, since STL is a property specification language, this framework can be applied to analyze other properties of the system, not necessarily relying on snap-action.

Even if using STL diagrams can be seen as improvements of DLE diagrams, they do not address all their limitations. In both cases, only two initial protein concentrations are modified (XIAP and caspase-3 in our examples). Therefore, they fail to capture all the differences between cell lines. In more precise terms, DLE and STL diagrams represent the value of the DLE and of an STL property in a 2D slice of the high-dimensional state space, and cell line distributions are projected onto the slice. Therefore, even if they provide insight into the behavior of cells that are affected by changes in initial protein concentrations, DLE and STL diagrams must be interpreted with care. The information is exact for the cell line used to construct the diagram, but it is only

approximate for other, projected cell lines. To investigate how the diagrams change when reference cell line changes, we constructed the Property 1 diagrams with respect to OE-Bcl2 HCT116, OE-Bcl2 SKW6.4, and OE-Bcl2 T47D cell lines (Figure S3A-C). Although the conclusions based on Figure 3 are indeed valid for HCT116 and SKW6.4 cell lines (OE-Bcl2 HCT116 cells survive, OE-Bcl2 SKW6.4 cells die), they differ for T47D cells. When using a slice of the state space based on OE-Bcl2 T47D cells, it appears that these cells are classified as exhibiting mixed-type behaviors (Figure S3C), as experimentally observed, instead of mostly type I as suggested by Figure 3. This example illustrate that problems may arise when placing different cell lines on the same phase diagram. To obtain a less comprehensive but more accurate view of the value of STL properties, we propose to use *STL population data* in combination with phase diagrams. To do so, we create *in silico* populations of cells for each given cell line by sampling lognormal distributions for *all* initial protein concentrations to mimic cell-to-cell variability. Their means correspond to nominal initial protein concentrations, and standard deviations are either set based on experimentally-measured coefficient of variations or are assumed to be 25% (see Methods, [5,19]). One can then evaluate property values for all these cells and compute statistics on these values such as the mean value, its standard deviation, or the percentage of satisfaction of the property (i.e. the percentage of cells in the population satisfying a given property). For Property 1, these statistics are presented in Figure 4 (and Figure S4 for all cell lines). One can first check that indeed the mean values, distributions and satisfaction rates of Property 1 are qualitatively consistent with the predictions we obtained from the STL diagram in Figure 3 for the OE-Bcl2 HCT116, OE-Bcl2 SKW6.4, OE-Bcl2 T47D, and OE-Bcl2/ΔXIAP HCT116 cells. Moreover, the satisfaction rates in Figure 4 can be directly compared with the experimentally-measured survival rates in clonogenic assays presented in Figure 2B and Figure 7C of Aldridge et al. (2011). Strikingly, our data shows excellent quantitative agreement with observed cell behaviors for all but the parental T47D cell line. Like in clonogenic assays, we predict the survival of a large majority of OE-Bcl2 HCT116 cells, half of the OE-Bcl2 T47D cells and a minority of HCT116 cells, the death of all ΔXIAP HCT116 and SKW6.4 cells and their OE-Bcl2 variants. The sole discrepancy concern T47D cells that are predicted to be more resistant to apoptosis than experimentally-observed.

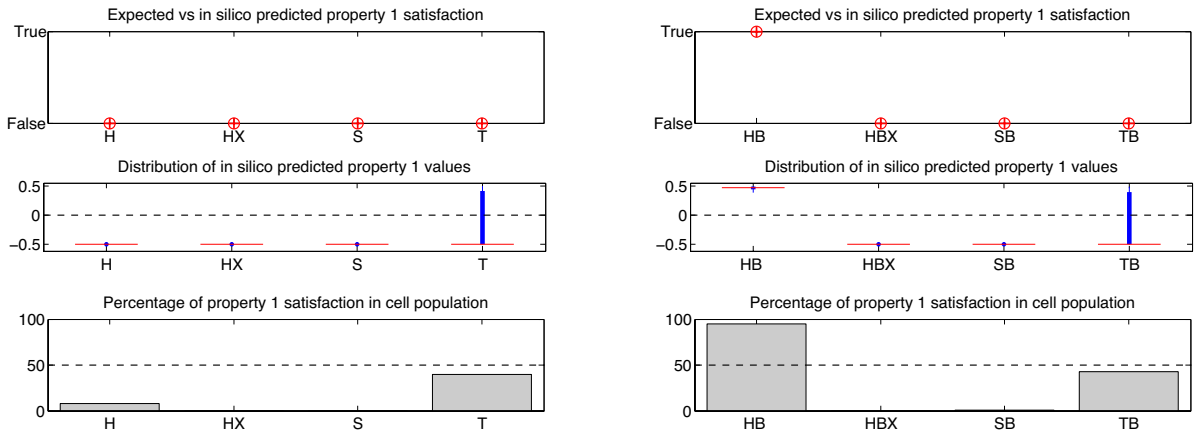

Figure 4: Property 1 population statistics. Plots indicate the nominal cell value (cross, top), the distribution (middle), and the percentage of satisfaction (bottom) of the values of Property 1 for populations of cells of different cell lines. For distributions, box boundaries and red line indicate first and third quartiles, and median, respectively. When experimental data is available, circles in the top plot represent the expected values. These statistics are computed for populations of 5000 cells. The following abbreviations are used in this and further figures: H is HCT116, HX is ΔXIAP HCT116, HB is OE-Bcl2 HCT116, HBX is OE-Bcl2/ΔXIAP HCT116, S is SKW6.4, SX is ΔXIAP SKW6.4, SB is OE-Bcl2 SKW6.4, SBX is OE-Bcl2/ΔXIAP SKW6.4, T is T47D, TX is ΔXIAP T47D, TB is OE-Bcl2 T47D and TBX is OE-Bcl2/ΔXIAP T47D.

Property 2: Activations of initiator and effector caspases are sequential in Type II cells

In addition to survival of derived cell lines overexpressing Bcl2, Scaffidi and colleagues observed another important difference between type I and II cell lines: the dynamics of the activations of initiator and effector

caspases by cleavage show marked differences [4]. These are two critical events that can be considered as markers of the beginning and of the end of the apoptosis decision-making process. By using Western blots, Scaffidi and colleagues showed that in type I cells the activation of the effector caspase caspase-3 closely follows the activation of the initiator caspase caspase-8: caspase activations are gradual and near synchronous. In contrast, in type II cells the activation of initiator caspases is not closely followed by the activation of effector caspases [4]. Similar results have been obtained with a cellular resolution using FACS analysis (Figure 5 of Aldridge et al. (2011). The current understanding is that effector caspase activation is delayed until MOMP happens. Hence, the observed sequential activation is explained by a pre-MOMP delay in type II cells. Therefore this synchronous vs. sequential activation is not only a robustly observed pattern but also relates to mechanistic interpretation of cell death.

In Aldridge et al. (2011), the caspases activations are followed by flow cytometry measurements detecting the presence of cleaved substrates of caspases-8 and -3. Here, we will consider that initiator and effector caspases activations are sequential if they are separated by more than one hour, in accordance with the low-temporal resolution observations made in Scaffidi et al. (1998) and Aldridge et al. (2011). So to express sequential activation, we say that "at some time point, caspase-8 is active and for at least an hour, caspase-3 remains inactive". Hence, we have the following STL formula: $Property2:= eventually(Casp8_{active}$ and $always_{[0\text{-}1h]}$ not $Casp3_{active})$. We still have to set the threshold concentration for cleaved caspases that corresponds to a detectable activity. Since it has been shown that caspases are highly potent proteases (a few hundred caspases can cleave millions of substrate proteins within hours [47,48], we set this threshold concentration to 1% of the total caspase concentration: $Casp8_{active}:= Casp8^*/Casp8_{total}>1\%$, and $Casp3_{active}:= Casp3^*/Casp3_{total}>1\%$ where $Casp8^*$ and $Casp3^*$ are the sum of the concentrations of all cleaved forms of caspase-8 and caspase-3, with the exclusion of caspase-8 bound to Bar and of caspase-3 bound to XIAP, respectively (the influence of the threshold is discussed in Figure S1).

Having formalized our property in STL, one can automatically construct the corresponding diagram (Figure 5, left). On this diagram one can clearly see two distinct, positive and negative, regions. HCT116 and T47D cells lie in the positive region and hence are predicted to satisfy Property 2, whereas SKW6.4 cells lie on the separatrix, and hence are predicted to show a mixed phenotype with respect to Property 2. The diagram also predicts that ΔXIAP mutants violate Property 2 (i.e. lie in the negative region). The predicted phenotypes of HCT116 and of ΔXIAP HCT116 cells are consistent with observations: whereas HCT116 cells show a clear sequential activation of caspases, this behavior is lost in ΔXIAP HCT116 cells [5]. Diagram shows that the EARM1.4 is also compatible with the hypothesis that high levels of XIAP control caspase activation and substrate cleavage, and may promote apoptosis resistance and sublethal caspase activation *in vivo* [16]. However, the predicted phenotype of SKW6.4 cells is in contradiction with the observed one: as expected from type I cells, SKW6.4 cells clearly show synchronous activations of caspases. The analysis of the OE-Bcl2 mutants of the HCT116, ΔXIAP HCT116, and SKW6.4 cell lines shows that consistent results are obtained in these cases (Figure 5, right). One should note that because caspase-3 is not activated in OE-Bcl2 HCT116 cells (they survive TRAIL treatment), Property 2 holds trivially in these cells. To investigate whether EARM1.4 can account for the observed phenotype of SKW6.4 cells, we slightly relaxed the timing constraint between the caspases activation times and found that by setting a slightly longer delay (e.g. 1h30min), the mean value of Property 2 for the SKW6.4 cell population becomes negative as expected, and even more, that the percentage of cells satisfying Property 2 decreases to zero with longer delays. Therefore we conclude that the observed discrepancy results from EARM 1.4 limitations to capture quantitatively the elapse of time between events, rather than from severe modeling flaws.

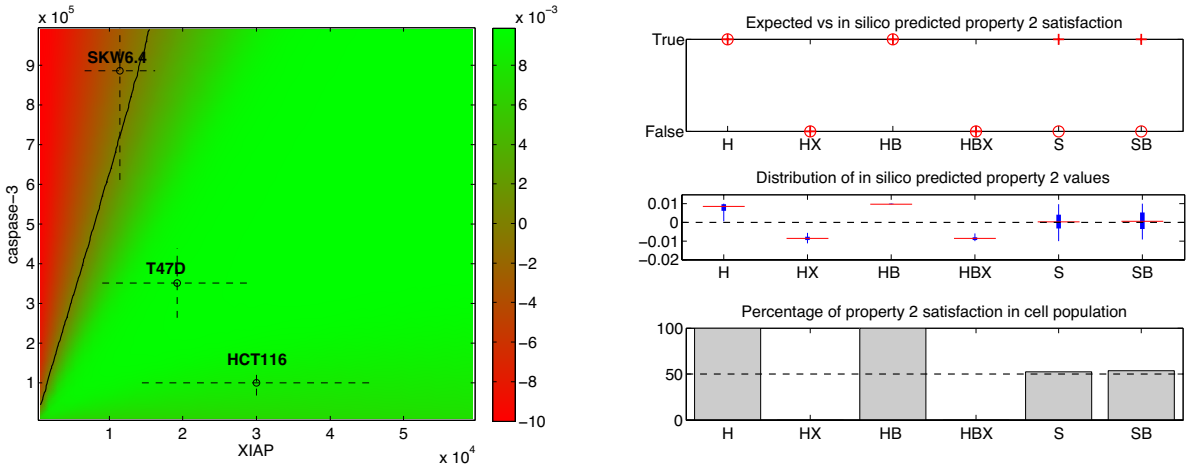

Figure 5. Property-2 phase diagram and statistics. Left: the value of Property 2 (*p2:= eventually(Casp8$_{active}$ and always$_{[0-1h]}$ not Casp3$_{active}$)*) is represented as a function of the XIAP and caspase-3 initial concentrations. As in Figure 3, cell lines are positioned in this diagram according to their protein initial concentrations. Right: distributions of the values of Property 2 across populations of cells of different cell lines. Notations are identical to those used in Figure 4. One can note that there is a discrepancy between the (positive) predicted mean value of Property 2 for SKW6.4 cells and experimental observations (Property 2 not satisfied).

Property 3: MOMP precedes caspase-3 activation in Type II cells

In type I and type II cells, MOMP happens during apoptosis with comparable kinetics [4]. This is in apparent contradiction with the very different role of MOMP in the two pathways, as revealed by Bcl2 overexpression experiments (see Property 1 paragraph), and with the different kinetics of caspases activations (see Property 2 paragraph). The current understanding is that in type I cells MOMP is a consequence of effector caspases activation, whereas in type II cells, MOMP is the cause of effector caspases activation [4,8,49]. Under this assumption one should observe that in the first case MOMP follows effector caspases activation, and in the second case, that MOMP precedes effector caspases activation. This question has been directly investigated in Aldridge et al. (2011) by staining cells with anti-cytochrome c and anti-cPARP antibodies. The authors demonstrate that most of HCT116 cells showing effector caspases activation also show cytoplasmic cytochrome c localization. Stated differently, caspase-3 is not active until MOMP happens. This is not always true for ΔXIAP HCT116 cells, or for OE-Bcl2 ΔXIAP HCT116 cells: a significant proportion (respectively 20% and 80% of the cells) shows effector caspase activation in absence of cytoplasmic cytochrome c (Figure 3 of [5]). The same experiment was made for T47D and OE-Bcl2 T47D cells, showing that these cells behave like HCT116 cells: caspase-3 is not active until MOMP happens (Figure 7 of [5]).

To test the consistency of EARM1.4 with these observations, we express in STL the property, typical of type II behaviors, that cells remain alive until MOMP happens. We simply write *Property3:= MOMP release alive,* with *alive:= cPARP/PARP$_{total}$<0.5* as in Property 1. The *release* operator states that the second property (*alive*) must hold until the first property holds for the first time (*MOMP*). The occurrence of MOMP is detected by the titration of Apaf-1 by the released cytochrome c to form the apoptosome. We say that MOMP happened when more than 50% of Apaf-1 is bound to cytochrome c: *MOMP:= Apaf$_{free}$/Apaf$_{total}$<0.5* (see Figure S1 for discussion of threshold). Then, we used Breach to compute the STL diagram associated with Property 3 with respect to HCT116 cells, and the Property 3 population data (Figure 6). One should note that like in the *in vitro* setup of Aldridge and colleagues (2011), only cells in which MOMP happened were taken into account: we excluded surviving cells to compute statistics.

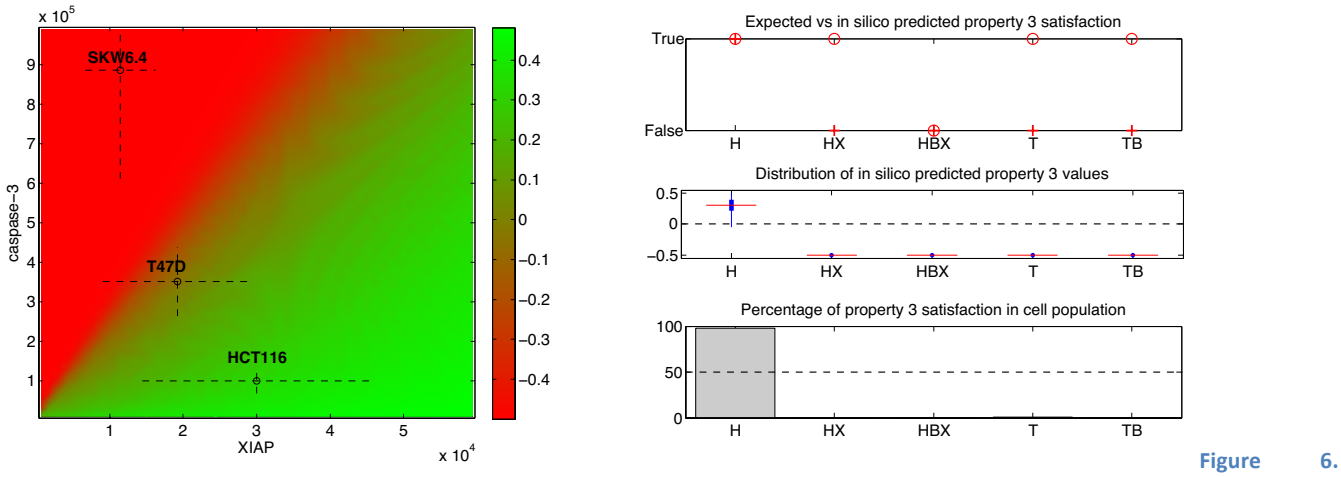

Figure 6. Property-3 phase diagram and statistics. The value of Property 3 (*p3:= MOMP release alive; p3:= $Apaf_{free}/Apaf_{total}$<0.5 release (cPARP/$PARP_{total}$< 0.5)*) is represented as a function of the XIAP and caspase-3 initial concentrations. As in Figure 3, cell lines are positioned in this diagram according to their protein initial concentrations. One can see on this diagram that HCT116 depleted from all XIAP ([XIAP]=0) are predicted not to satisfy Property 3, in contradiction to experimental observations. The minimal XIAP concentration for which a large proportion of HCT116 cells still satisfy Property 3 is around 10^4 molecules, corresponding to the inactivation of at most two thirds of XIAP activity in ΔXIAP HCT116 cells. (Right) Distributions of the values of Property 3 across populations of cells of different cell lines. Notations are identical to those used in Figure 4. One can note that discrepancies between predicted mean values and observed phenotypes exist for ΔXIAP HCT116, T47D and OE-Bcl2 T47D cells.

The diagram presented in Figure 6 is consistent with the observation that HCT116 cells satisfy the property. However, it suggests that the ΔXIAP mutant falsify the property, since negative values are found in the region where XIAP concentration is null. This is in contradiction with the observation that caspase-3 is active before MOMP happened in a majority (80%) of these cells. Also contradictions are found with T47D, and OE-Bcl2 T47D cells (Figure 6, right). The fact that ΔXIAP HCT116 cells have been observed to satisfy Property 3 but not Property 2 imposes strong constraints on the kinetics of the apoptosis process. In these cells, caspase-3 activation is precocious, since it follows by less than one hour the activation of caspase-8, implying that death (i.e. PARP cleavage) is rapid since it follows shortly after caspase-3 activation. But then Property 3 implies that MOMP happened even before this time instant. Given the efficient caspase-3 activation in EARM1.4, the model fails to capture the need for MOMP in these cells. Although ΔXIAP HCT116 cells present a type I phenotype with respect to clonogenic survival and caspases activation dynamics, and a type II phenotype with respect to the need for MOMP for cell death, the model consistently classifies these cells as type I cells.

Improving EARM 1.4: Property-guided parameter search

In summary, we found that EARM1.4 satisfies the majority of the observed behaviors encoded in STL (Table 1). This is commendable for a model of this size and complexity, given that EARM1.4 has not been tuned with respect to these properties, even if the model and the specific observations we used to state our STL properties have been published in the same paper. However, few discrepancies were identified. It is important to test whether the proposed model is structurally not capable of accounting for all the observed properties. If not, this would call for significant model revision.

Cell line \ Property	Property 1	Property 2	Property 3
HCT116	False	True	True
ΔXIAP HCT116	False	False	**True**
OE-Bcl2 HCT116	True	True	N/A
OE-Bcl2 ΔXIAP HCT116	False	False	False
SKW6.4	False	**False**	N/A
OE-Bcl2 SKW6.4	False	**False**	N/A
T47D	False	N/A	**True**
OE-Bcl2 T47D	Mixed	N/A	**True**

Table 1: Summary of findings. Truth values of the three properties as observed in Aldridge et al. (2011) for the HCT116, SKW6.4, and T47D cell lines and some mutants. N/A indicates that the experimental information is not available. Experiments showed that OE-Bcl2 T47D cells present clonogenic survival rates close to 50%, hence their "mixed" behavior. Discrepancies obtained with the original EARM 1.4 model are highlighted in bold. $p1 := always_{[0\text{-}6h]}(alive)$; p2:= $eventually(Casp8_{active}\ and\ always_{[0\text{-}1h]}\ not\ Casp3_{active})$; $p3 := MOMP\ release\ alive$. Because of their ambiguous phenotypes, T47D cell data (in grey) were not used for parameter search.

We first tried to resolve inconsistencies by minor adjustments of the thresholds we used in formulae. However, property satisfaction values proved robust to threshold changes (Figure S5). We therefore resorted to search for better parameter values using global optimization methods [50]. We defined a cost function that indicates for any given parameter how far the model is from satisfying all its constraints. More precisely, the cost function aggregated three measures: how many properties are consistent with the observations, how robustly satisfied or falsified they are, and how large are the deviations of the parameters with respect to their reference values. Then, we used the global optimization tool CMA-ES [51] to search automatically for parameters minimizing this cost function. The parameter search procedure is described in details in the Method section. Here, one should note that the real-valued semantics of STL properties is critical: continuous optimization tools take advantage of the graded interpretation of STL properties, whose values indicate their "distances from satisfaction". The sole use of traditional Boolean-valued interpretation of temporal logic formulae would have made this search impractical. Because of their ambiguous phenotypes, T47D cell data were not used for parameter search. We started with 43 parameters, that is, all catalytic and forward reaction rates (see Method section). After applying our optimization procedure we found that the modification of only 2 parameters was sufficient to achieve full agreement with experimental data. The parameters found by the search procedure are a parameter regulating the strength of the caspases feedback loop (2.71 fold increase) and a parameter regulating the kinetics of PARP cleavage (55.6 fold decrease) (Table S1). Given the usually large uncertainties in actual parameter values, such changes can still be considered as acceptable. New parameter values lead to satisfaction of Property 1-3 in *nominal* cells corresponding to all HCT116 and SKW6.4 normal and derived cell lines. To test whether property values are corrected at the *cell population* level, we recomputed the population data with these new parameter values. As shown in Figure 7, all inconsistencies were indeed resolved at the cell population level for all cell types (again with the exception of T47D cells). We note that T47D cells still do not satisfy Property 3 (Figure 7 and Figure S5).

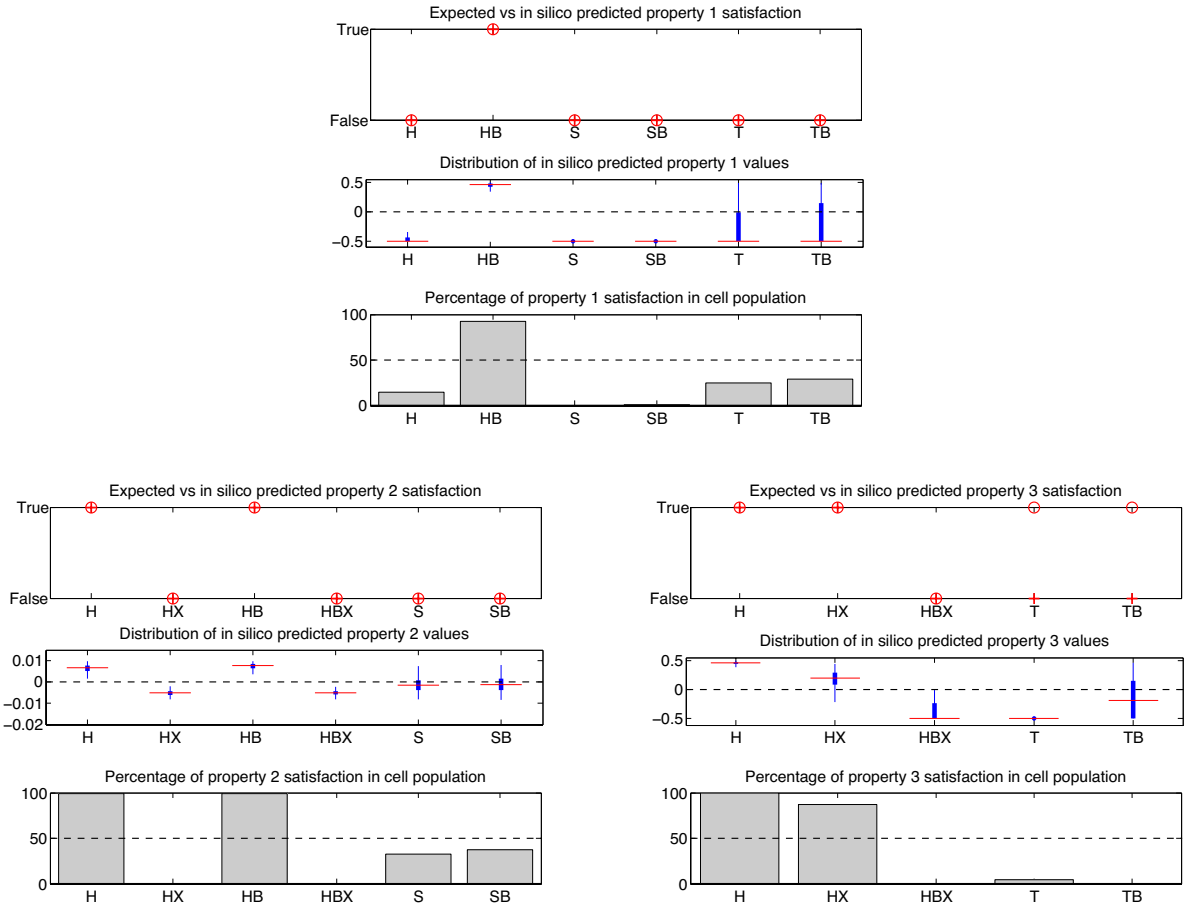

Figure 7: Population statistics for updated EARM1.4 model. Population statistics for Property 1, 2 and 3, computed with new parameter values (Table S1). The new parameter values allow resolving the inconsistencies found for SKW6.4, OEBcl2 SKW6.4 cells for Property 2, and for ΔXIAP HCT116 cells for Property 3. T47D cells still do not satisfy Property 3.

Origins of type I/II behaviors: key role of downstream proteins and of a positive feedback loop

It is important to note that the significantly different phenotypic responses of the different cell lines are in the model solely explained by taking into account observed differences in the initial concentrations of a dozen of key proteins. No parameter needs to be changed. Therefore one can use EARM1.4 with new parameter values (Table S1) and STL diagrams to investigate the *origins* of the different behaviors shown by cell lines. As noted by Aldridge et al. (2011), one important question is to distinguish whether the different behaviors can be explained exclusively by differences in upstream protein concentrations or exclusively by differences in downstream protein concentrations, or whether a combination of upstream and downstream changes is needed. Indeed, it has been proposed that the main differences between type I and II behaviors are essentially due to differences in efficiency of the initiator caspase activation by the DISC [4,8,52]. It has also been proposed that the main determinant is the XIAP concentration relative to caspase-3 [3,5]. As apparent in the Property 2 diagram (Figure 5), and as also mentioned in Aldridge et al. (2011) based on DLE diagrams, it is clear that differences in XIAP or caspase-3 levels, that is, in downstream protein concentrations, can explain the observed differences for HCT116 and SKW6.4 cell lines. To investigate whether FLIP and caspase-8 levels, the sole upstream proteins which initial concentrations change for different cell lines in EARM1.4, may explain the observed differences between cell types, we computed the STL diagrams showing the effects of changes in FLIP or caspase-8 levels (Figure 8A). As apparent on the diagram, changing FLIP and caspase-8 levels in HCT116 cell line to match the

levels found in the other cell type does not affect the Property 2 values (i.e. Property 2 in Figure 8A is positive for HCT116 even if we use Caspase-8 and FLIP levels as measured in SKW6.4 or T47D cells). Note that using STL was instrumental here, since the corresponding DLE diagram does not offer intuitive interpretation (Figure 8B). This lack of influence of any upstream protein concentration is in apparent contradiction with the markedly different profiles for caspase-8 activation observed experimentally in Scaffidi et al. (1998) between type I and type II cells, and in EARM1.4 between HCT116 and SKW6.4 cell lines (Figure 8C and 8D), and even more between normal and ΔXIAP cells that differ only in XIAP concentration (Figure 8C and 8D). The latter comparison suggests, for both HCT116 and SKW6.4 cell lines, that differences in downstream protein concentrations (e.g. XIAP) feed back on upstream protein activities (caspase-8 in this case). Indeed, the *in silico* inactivation of the positive feedback loop of caspase-3 on caspase-8 in HCT116 and SKW6.4 cells, obtained by zeroing the cleaveage rate of caspase-8 by caspase-6 (denoted ΔFB cells), leads to similar activation profiles for caspase-8 in the two cell lines (Figure 8C and 8D). Note that cells still undergo apoptosis (Figure 8C and 8D, lower plots), but in a delayed manner, that is in agreement with the findings of Albeck et al. (2006). Extending this view, our result suggest, that the strength of the caspase feedback loop influences not only the timing of death, but is also required to correctly reproduce Property 2 in type I and II cell lines. Indeed, when the feedback is removed, type I cells loose their Property 2 characteristics (Figure S6). We conclude that based on the EARM1.4 model predictions, one can reconciliate the different views expressed by Scaffidi et al. (1998) and by Aldridge et al. (2011). There are indeed functionally significant differences in upstream protein activities (e.g. caspase-8) in type I and II cells. However, according to EARM1.4 model, these differences do not result from differences in upstream protein levels but rather from downstream differences (XIAP and caspase-3) that feed back their influence on upstream processes. The feedback is also required to preserve synchronous initiator and effector caspase activation in type I cells.

The analysis of the FLIP/caspase-8 STL diagrams for Property 2 and 3 reveals that moderate inhibition of caspase-8 levels in SKW6.4 cells would transform them into cells showing mixed type behaviors (Figure S7). Indeed the model predicts that these cells would present a sequential activation of caspases (Property 2 satisfied; a type II feature) and a MOMP-independent death (Property 3 violated; a type I feature). This mutant would show exactly the opposite behavior of ΔXIAP HCT116 cells, a combination of behaviors that has not yet been observed. Therefore, the detailed analysis of this cell line could possibly provide a valuable information on the interplay between the two apoptotic pathways. Similarly, the partial inhibition of caspase-3 levels in SKW6.4 cells would also lead to cells showing mixed type behaviors (p1 remains false whereas p2 and p3 change to true; Figure S8).

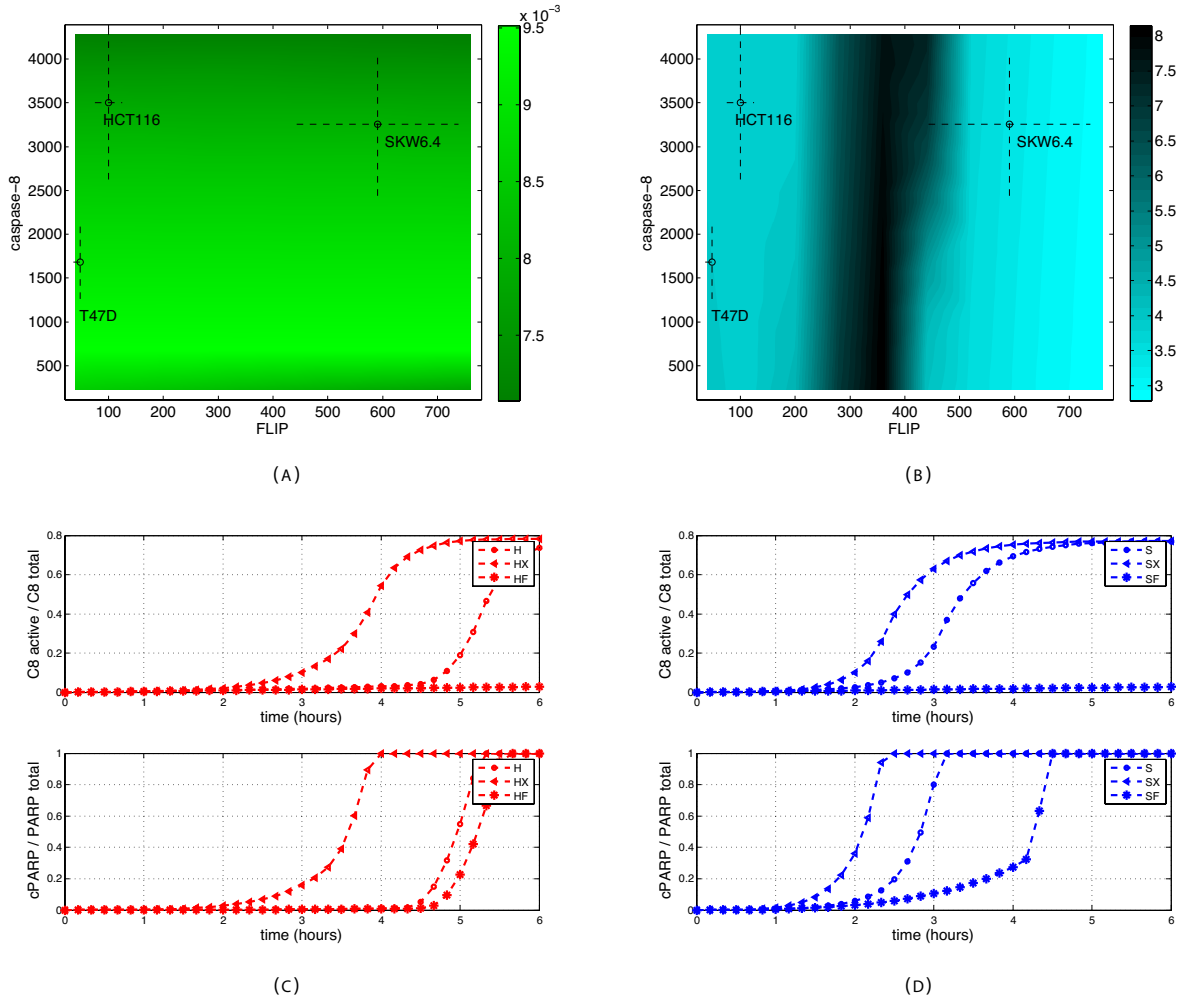

Figure 8. Investigating the role of upstream proteins. (A) STL and DLE diagrams showing Property 2 values as a function of FLIP and caspase-8 initial concentrations. Other protein concentrations correspond to nominal protein concentrations for HCT116 cells. We observe that changing FLIP or caspase-8 levels in HCT116 cells to match the levels found in the other cell types does not affect Property 2 satisfaction. (B) The corresponding DLE diagram does not offer intuitive interpretation. (C and D) Temporal evolution of active caspase-8 (top) and cleaved PARP (bottom) in HCT116 cells (red circle), SKW6.4 cells (blue circle), ΔXIAP HCT116 cells (red triangle), ΔXIAP SKW6.4 cells (blue triangle), ΔFB HCT116 (red star) and ΔFB SKW6.4 cells (blue star). The comparison of HCT116 and SKW6.4 cell lines with their ΔXIAP mutant shows important differences in the caspase-8 activation profile. Downstream proteins change upstream protein activation.

Discussion

In this work, we expressed in a formal language, STL, a number of observed properties on molecular details of extrinsic apoptosis in several mammalian cell lines, and systematically tested their consistency with a previously-proposed model developed to capture the same process in the same cell lines, EARM1.4 [5]. It is important to note that even if model and experimental data have been published in the same article, the model has not been tuned to comply with the various properties we tested on the different cell lines. Indeed, we found several inconsistencies between model predictions and experimental observations. These inconsistencies can be resolved by model reparametrization involving a limited number of parameter changes. However, these needed changes were affecting key processes, namely the PARP cleavage rate and the strength of the caspases-3, -6 and -8 feedback loop. It is remarkable that the model was able to explain a number of experiments probing different aspect of apoptosis made on different cell lines and mutants, simply by taking into account observed differences in protein concentrations but keeping the same model structure and reaction rates for all cell lines. This makes it a valuable tool to investigate the *origins* of the two different cell responses. Unlike in *in vivo* experiments, the

number of factors that could explain these differences is limited in EARM1.4. Using STL diagrams, we showed that observed differences in the concentrations of upstream proteins in different cell lines could not account for the observed cell type changes. This finding is consistent with the observation that downstream proteins, most notably XIAP and caspase-3, play a key role, made by Aldridge et al. (2011) and based on *in vivo* and *in silico* works, but is in apparent contradiction with the observation that upstream protein activities are markedly different in type I and II cell lines, made by Scaffidi et al. (1998). Detailed analysis showed that the effects of downstream protein concentration differences are in fact fed back to upstream processes and amplified via the positive feedback loop involving caspases 3, 6, and 8. This finding reconciliate the views expressed by Scaffidi et al. (1998) and Aldridge et al. (2011).

Based on experimental observations, we defined three properties associated with type II behaviors: the cell survives if Bcl2 is over-expressed, the activations of initiator and effector caspases are sequential, and MOMP precedes caspase-3 activation. They all assess the role of mitochondria for cell death and differ only in subtle means. However, they are not always equivalent. For example, ΔXIAP HCT116 cells satisfy Property 3 but not Property 2, leading to interpretations like ΔXIAP HCT116 being type I cells while exhibiting a type II phenotype. Based on our work, there is no evidence that one property could be considered as a defining criterion, excepted maybe for historical or practical reasons (cell types were originally defined based on caspase activation kinetics whereas Bcl2 overexpression is considered as the standard method for cell type classification). This challenges the consensual understanding that there exists (implicitly) well-defined type I and type II phenotypes. It should be noted that here we go beyond the notion of mixed cell type introduced by Aldridge and colleagues for describing T47D cells. The authors implicitly assume that cell types are well defined but that within a population of cells a mixture of both phenotypes can be observed, coming from cell-to-cell variability [6,7,19]. Here we propose that these three properties are considered as *type II features*. Then the ΔXIAP HCT116 cells would be more consistently qualified as possessing some type I and some type II features. With the accumulation of more detailed characterizations of apoptosis in more cell lines, it is likely that the use of the loosely-defined notion of cell types will otherwise become more and more problematic.

Like the DLE diagrams introduced in Aldridge and Haller (2006), STL diagrams are a convenient and intuitive way to represent the influence of various factors on complex dynamical properties. However, STL diagrams are superior on several counts. Firstly, one can benefit from the expressive power of temporal logics to express different observed properties of the dynamics of the cell response. Secondly, the evaluation of STL properties and of the DLE returns continuous values. However, the fact that STL values are signed – positive values indicate satisfaction and negative values indicate falsity – allows for a more direct interpretation of the diagrams (Figure 8). Thirdly, DLE generates well-defined partitions if in some regions a small change in the initial state has a mild effect on the future system's state, thus generating low DLE values, and in other regions, similar changes have drastic effects, thus generating high DLE values. Although this is clearly the case in cell lines overexpressing Bcl2 since some cells die, whereas others survive (Figure 3), this is not generally true (Figure 8).

DLE and STL diagrams are particularly useful to have a rapid view of the consequences of changing a few factors, initial concentrations in our case. This feature allows us to foresee the consequences of mutations (e.g. ΔXIAP mutants in XIAP/caspase-3 diagrams), to investigate the (lack of) influence of given factors (e.g. FLIP changes in FLIP/caspase-8 diagrams), and to assess the influence of cell-to-cell heterogeneity by representing graphically the means and standard values of populations in diagrams. However, heterogeneity in diagrams is limited to two dimensions. Moreover, since the cell lines differ in more than two dimensions, only one cell line can be correctly mapped in the state space slice of the diagram. Other cell lines are projected onto it, making their interpretations subject to caution. To solve this issue, we introduced population property values for describing the behavior of cell populations. These values and their statistics, notably means, standard deviations, and

percentage of satisfaction, offer a more accurate view than phase diagrams. Indeed, even if we found that the rapid picture offered by STL diagrams are often consistent with population property values, a few cases illustrated the need to compute these statistics as well (e.g. T47D cells manifesting *in silico* a clear mixed-type behavior with respect to Property 1, that is not present in the phase diagram in Figure 3).

In addition to computing diagram and population statistics, STL properties also enable model revision based on *experimental observations*. Observed properties are encoded in STL and the continuous semantics of STL is used to search for valid parameter values. Traditional model revision methods based on curve fitting could not be adapted here by lack of well-defined time series data. The non-standard use of continuous semantics for temporal logic formula interpretation is essential to allow for an effective search [46,53,54]. Using global optimization methods, we found that the few discrepancies we had identified in earlier steps can be resolved by modifying only a restricted set of model parameters. Remarkably, one of the two selected parameters is regulating the strength of the caspases feedback loop, a processes that is predicted to play an important role in the genesis of type I or type II behaviors.

The development of experimental methods to probe quantitatively subtle aspects of the dynamics of biological processes has spurred the development of large and complex quantitative models [55,56]. However the available experimental data is seldom in the form of time series data directly usable by standard model validation and model calibration techniques. Therefore tools allowing for the exploration of model properties, the comparison between predictions and observations and the revision of models that are adapted to the available experimental data are increasingly needed. Temporal logics offer a flexible means to encode for a broad range of experimentally-observed properties. Moreover they are also formal languages that allow automating model analysis. Because it supports STL and uses by default distributions for parameter and initial concentrations, Breach naturally allows the exploration of properties of cell populations. We expect that Breach will become a valuable tool for the computational biologists to explore model properties, and more importantly, to get tight connections between experimental data and model predictions [57].

Methods

Modeling extrinsic apoptosis and cell line differences. We used the model of extrinsic apoptosis proposed by Aldridge and colleagues (2011) named EARM1.4. This model is an extension and adaptation of a previous model, EARM1.0, proposed in [18]. This model has been calibrated on HeLa cells using live and fixed cell imaging, flow cytometry of caspases substrates and biochemical analysis. EARM1.4 has been adapted to HCT116, SKW6.4 and T47D cells, and has been shown to capture their capacity to die or survive in OE-Bcl2 experiments. It is a mass-action ODE model based on nearly 70 reactions and involving 17 native proteins, 40 modified proteins or protein complexes, and TRAIL. For each cell line, the model assumes different nominal initial protein concentrations. Nominal concentrations refer here to concentrations found in a hypothetical mean cell within the cell population. More precisely, out of the 17 native proteins, 12 have been quantified by immunoblotting and the relative differences between cell lines have been used to set nominal initial protein concentrations for HCT116, SKW6.4 and T47D cells (see Table 2). Besides initial concentrations, the 3 models are identical. ΔXIAP and OEBcl2 mutant cell lines are defined with respect to their parent cell line. In ΔXIAP cells, the XIAP concentration is set to 0. In OE-Bcl2 cells, the initial Bcl2 concentration is 10 times higher than in the parent cell line. For cells with modified feedback (ΔFB cells) we set k7 to 0. To represent cell-to-cell variability within cell lines, we assumed that protein concentrations are log-normally distributed. The means of protein concentrations were the nominal values. The coefficient of variation were either measured, for caspase-3 and XIAP [5], or assumed to be 25% as in [19]. The complete model together with Breach is available in Supplementary Materials as MATLAB file (S9). The names of the variables, constants and reactions used in the model are the same as in the EARM1.4 [5].

Protein \ Cell line	HCT116	SKW6.4	T47D
FLIP	100 (0.25)	591 (0.25)	48 (0.25)
caspase-8	3500 (0.25)	3255 (0.25)	1680 (0.25)
caspase-6	10000 (0.25)	6700 (0.25)	22500 (0.25)
caspase-3	100000 (**0.32**)	886000 (**0.31**)	351000 (**0.25**)
XIAP	30000 (**0.52**)	11400 (**0.42**)	19200 (**0.53**)
PARP	1000000 (0.25)	1120000 (0.25)	1040000 (0.25)
Bid	40000 (0.25)	74800 (0.25)	53600 (0.25)
Mcl1	1000 (0.25)	1250 (0.25)	4640 (0.25)
Bax	80000 (0.25)	786400 (0.25)	113600 (0.25)
Bcl2	20000 (0.25)	400000 (0.25)	104000 (0.25)
Smac	100000 (0.25)	177000 (0.25)	139000 (0.25)

Table 2. Initial concentrations of proteins in parental cell lines. Nominal values and coefficients of variations for initial protein concentrations that differ between cell lines. The relative abundance of proteins in different cell lines was set based on quantitative immunoblotting, and the coefficients of variations for caspase-3 and XIAP (bold) were determined based on flow cytometry measurements [5]. The coefficients of variations of all other proteins have been set to 25% as in [19].

Evaluation of properties in STL. Observed properties are expressed in STL. STL is an intuitive yet formal language for specifying the properties of continuous dynamical systems. Here we provide an intuitive introduction to the syntax and semantics of STL. A formal description can be found in [28]. Here, our STL properties were based on simple expressions on protein concentrations, like $cPARP < 10^5$,or on time like $time < 1h$. These properties can be combined using traditional logical operators, like *and, or* and *implies*, and using temporal operators, like *eventually, always*, and *until*. The scope of temporal operator can be limited by times expressions. These operators can be combined to create properties of arbitrary complexities. For example, $always_{<6h}(XIAP > 10^3 \text{ and } cPARP < 10^5)$ is a valid STL formula. STL properties are evaluated on simulation trajectories. STL properties have two possible interpretations: Boolean or continuous. The Boolean interpretation is fairly intuitive. The property $cPARP < 10^5$ is true at some time instant t if the value of the variable for cPARP is higher than 10^5 at time t. The property $XIAP > 10^3 \text{ and } cPARP < 10^5$ holds at all time points where both operands are true. At time t, $always(XIAP > 10^3)$ holds if $XIAP > 10^3$ holds at all future time instants t', $t'>t$. $always_{<6h}(XIAP > 10^3)$ holds if $XIAP > 10^3$ is continuously true during the next 6 hours. Lastly, $eventually(XIAP > 10^3)$ holds if at some future time $XIAP > 10^3$ holds, and $XIAP > 10^3 \text{ until } cPARP < 10^5$ holds if $cPARP < 10^5$ is eventually satisfied and until this time, $XIAP > 10^3$ holds. The continuous interpretation of STL is based on the notion of distance from satisfaction. For example, the value of $XIAP > 10^3$ is simply the value of $XIAP - 10^3$. Trivially it is positive if $XIAP > 10^3$, and negative if $XIAP < 10^3$. The value of $XIAP > 10^3 \text{ and } cPARP < 10^5$ is the maximum of the value of the two operands. Note that it is positive if and only if both operands have positive value. Similarly, the value of $always(XIAP > 10^3)$ is the maximum of the value of $XIAP > 10^3$ at all future time instants. More generally, the continuous interpretation of STL properties ensures that if the value of a property is positive (resp. negative), then the property holds (resp. is violated) in the more usual Boolean interpretation. Moreover, it captures a notion of "distance from satisfaction": a large positive value indicates a robustly satisfied property, whereas a large negative value indicates a property that is far from satisfaction. However property values are relative to the property, in the sense that values obtained for different STL properties are not directly comparable between each other.

Computation of property diagrams and population data. Diagrams represent 2D slices of a high dimensional state space. Boundaries were set so as to enclose the variability observed between cell lines. The ranges for caspase-3, XIAP, caspase-8 and FLIP are [0, 10^6], [0, $6*10^4$], [1200, 4500] and [0, 800], respectively. Diagrams are defined with respect to a particular cell line: with the exception of the two variables of the diagram, all other

variables assume their nominal values for the given cell line. In practice, a 50x50 grid of linearly-spaced points is used for the computation of each diagram. STL diagrams represent the continuous values of an STL property evaluated on the simulated trajectories corresponding to all possible initial concentrations. DLE diagrams represent the direct finite-time Lyapunov exponent, computed at a given time (6 or 4 hours). This value captures the sensitivity to initial conditions: $DLE(t, x_0) = \log \lambda_{\{max\}} \left((\frac{\partial x(t)}{\partial x_0})^T (\frac{\partial x(t)}{\partial x_0}) \right)$, where $\lambda_{\{max\}}(M)$ denotes the maximum eigenvalue of the matrix M. For STL population data, 5000 different initial conditions are obtained for each cell line by sampling around its nominal initial conditions from lognormal distributions. For each sampled initial condition, the behavior of the system is predicted by numerical simulation and the value of STL properties is evaluated. Mean values, value distributions and percentages of satisfaction of the property (based on Boolean interpretation) are represented.

Parameter search procedure. The search procedure has two phases. In the first phase we search for new parameters for EARM1.4 that lead to full agreement with experimental data (Table 1). In the second phase, when a solution is found, we minimize the number of modified parameters. We use a cost function composed of three different components: continuous, Boolean, and parameter penalties. The continuous penalties correspond to the (negation of) the STL continuous values, and the Boolean penalties correspond to their Boolean value multiplied by a (negative) constant. These costs decrease when more properties are consistent with observations ($B_{penalty}$), and when they are more robustly consistent with observations ($C_{penalty}$). In the continuous component, weights are used to balance the importance of all properties, given their typical range. The last component penalizes parameter deviations from their original values ($P_{penalty}$). The overall cost is the weighted sum of these three components.

$$cost(x) \coloneqq \alpha P_{penalty}(x) + \sum_{i \in CellLines} \sum_{p \in Properties} \left(\beta B_{penalty}(x, i, p) + \gamma C_{penalty}(x, i, p) \right)$$

In the first phase, we selected 43 parameters (14 catalytic rates of enzymatic reactions and 29 forward rates) out of approximately 80 parameters in EARM1.4. Parameter modifications were limited to a 100-fold change. We set weights so that the Boolean, continuous, and parameter penalties contributed to approximately 50%, 30%, and 20% of the cost, respectively. After 10 hours of computations (2.2GHz processor, 8GB RAM), the search converged to a state in which all expected properties were satisfied by the model (T47D cells excluded).

In the second phase, we selected the parameters that changed by more than 5 folds (there were 5 such parameters: kc9, kc25, kc20, k7 and k24) and run the search again for each pair of these parameters. The cost function was modified by setting the $C_{penalty}$ parameter to 0, and the beta parameter such as the Boolean penalty was responsible for approximately 90% of the cost. As a result, parameter deviations were minimized while preserving the agreement with the experimental data. We found that reparametrization of only one pair of parameters allowed for satisfaction of all tissues: a parameter regulating the strength of the caspases feedback loop and a parameter regulating the kinetics of PARP cleavage.

Breach tool. All the computations have been made using Breach [28,46]. This MATLAB/C++ toolbox allows for efficient numerical simulation, for sensitivity computation, and for STL property and DLE evaluation. In particular, DLEs can efficiently be computed via forward sensitivity analysis [58]. Breach is particularly oriented towards the analysis of parametric system, in the sense that it offers efficient routines for global sensitivity analysis and parameter search, and that the graphical user interface facilitates the modification of parameters and initial conditions, and the exploration of parameter spaces.

Acknowledgements

We thank Denis Thieffry, Magdalena Stepien and Xavier Duportet for their critical suggestions. This work was supported by the research grant Syne2arti ANR-10-COSINUS-007 from the French National Research Agency.

References

1. Gonzalvez F, Ashkenazi A (2010) New insights into apoptosis signaling by Apo2L/TRAIL. Oncogene 29: 4752–4765.

2. Spencer SL, Sorger PK (2011) Measuring and modeling apoptosis in single cells. Cell 144: 926–939.

3. Jost PJ, Grabow S, Gray D, McKenzie MD, Nachbur U, et al. (2009) XIAP discriminates between type I and type II FAS-induced apoptosis. Nature 460: 1035–1039.

4. Scaffidi C, Fulda S, Srinivasan A, Friesen C, Li F, et al. (1998) Two CD95 (APO-1/Fas) signaling pathways. The EMBO Journal 17: 1675–1687.

5. Aldridge BB, Gaudet S, Lauffenburger DA, Sorger PK (2011) Lyapunov exponents and phase diagrams reveal multi-factorial control over TRAIL-induced apoptosis. Molecular Systems Biology 7: 553.

6. Bhola PD, Simon SM (2009) Determinism and divergence of apoptosis susceptibility in mammalian cells. Journal of Cell Science 122: 4296–4302.

7. Rehm M, Huber HJ, Hellwig CT, Anguissola S, Dussmann H, et al. (2009) Dynamics of outer mitochondrial membrane permeabilization during apoptosis. Cell Death and Differentiation 16: 613–623.

8. Barnhart BC, Alappat EC, Peter ME (2003) The CD95 Type I/Type II model. Seminars in Immunology 15: 185–193.

9. Eissing T, Conzelmann H, Gilles ED, Allgöwer F, Bullinger E, et al. (2004) Bistability analyses of a caspase activation model for receptor-induced apoptosis. The Journal of Biological Chemistry 279: 36892–36897.

10. Klipp E, Liebermeister W, Wierling C, Kowald A, Lehrach H, et al. (2009) Systems Biology: A Textbook. 1st ed. Wiley-VCH.

11. Hoffmann A, Levchenko A, Scott ML, Baltimore D (2002) The IkappaB-NF-kappaB signaling module: temporal control and selective gene activation. Science 298: 1241–1245.

12. Bentele M, Lavrik I, Ulrich M, Stösser S, Heermann DW, et al. (2004) Mathematical modeling reveals threshold mechanism in CD95-induced apoptosis. The Journal of Cell Biology 166: 839–851.

13. Hua F, Cornejo MG, Cardone MH, Stokes CL, Lauffenburger DA (2005) Effects of Bcl-2 levels on Fas signaling-induced caspase-3 activation: molecular genetic tests of computational model predictions. Journal of Immunology 175: 985–995.

14. Bagci EZ, Vodovotz Y, Billiar TR, Ermentrout GB, Bahar I (2006) Bistability in apoptosis: roles of bax, bcl-2, and mitochondrial permeability transition pores. Biophysical Journal 90: 1546–1559.

15. Legewie S, Blüthgen N, Herzel H (2006) Mathematical modeling identifies inhibitors of apoptosis as mediators of positive feedback and bistability. PLoS Computational Biology 2: e120.

16. Rehm M, Huber HJ, Dussmann H, Prehn JHM (2006) Systems analysis of effector caspase activation and its control by X-linked inhibitor of apoptosis protein. The EMBO Journal 25: 4338–4349.

17. Chen C, Cui J, Lu H, Wang R, Zhang S, et al. (2007) Modeling of the Role of a Bax-Activation Switch in the Mitochondrial Apoptosis Decision. Biophysical Journal 92: 4304–4315.

18. Albeck JG, Burke JM, Spencer SL, Lauffenburger DA, Sorger PK (2008) Modeling a snap-action, variable-delay switch controlling extrinsic cell death. PLoS Biology 6: 2831–2852.

19. Spencer SL, Gaudet S, Albeck JG, Burke JM, Sorger PK (2009) Non-genetic origins of cell-to-cell variability in TRAIL-induced apoptosis. Nature 459: 428–432.

20. Fricker N, Beaudouin J, Richter P, Eils R, Krammer PH, et al. (2010) Model-based dissection of CD95 signaling dynamics reveals both a pro- and antiapoptotic role of c-FLIPL. The Journal of Cell Biology 190: 377–389.

21. Mai Z, Liu H (2009) Boolean network-based analysis of the apoptosis network: irreversible apoptosis and stable surviving. Journal of Theoretical Biology 259: 760–769.

22. Calzone L, Tournier L, Fourquet S, Thieffry D, Zhivotovsky B, et al. (2010) Mathematical modelling of cell-fate decision in response to death receptor engagement. PLoS Computational Biology 6: e1000702.

23. Saez-Rodriguez J, Alexopoulos LG, Zhang M, Morris MK, Lauffenburger DA, et al. (2011) Comparing signaling networks between normal and transformed hepatocytes using discrete logical models. Cancer Research 71: 5400–5411.

24. Schlatter R, Schmich K, Avalos Vizcarra I, Scheurich P, Sauter T, et al. (2009) ON/OFF and beyond--a boolean model of apoptosis. PLoS Computational Biology 5: e1000595.

25. Aldridge B, Haller G (2006) Direct Lyapunov exponent analysis enables parametric study of transient signalling governing cell behaviour. Systems Biology, IEE Proceedings 153: 425–432.

26. Algeciras-Schimnich A, Pietras EM, Barnhart BC, Legembre P, Vijayan S, et al. (2003) Two CD95 tumor classes with different sensitivities to antitumor drugs. Proceedings of the National Academy of Sciences of the United States of America 100: 11445–11450.

27. Ozören N, El-Deiry WS (2002) Defining characteristics of Types I and II apoptotic cells in response to TRAIL. Neoplasia 4: 551–557.

28. Donzé A (2010) Breach, a toolbox for verification and parameter synthesis of hybrid systems. Proceedings of the 22nd International Conference on Computer Aided Verification. Springer-Verlag. pp. 167–170.

29. Peter ME, Krammer PH (2003) The CD95(APO-1/Fas) DISC and beyond. Cell Death and Differentiation 10: 26–35.

30. Huang Y, Park YC, Rich RL, Segal D, Myszka DG, et al. (2001) Structural basis of caspase inhibition by XIAP: differential roles of the linker versus the BIR domain. Cell 104: 781–790.

31. Chen L, Smith L, Wang Z, Smith JB (2003) Preservation of caspase-3 subunits from degradation contributes to apoptosis evoked by lactacystin: any single lysine or lysine pair of the small subunit is sufficient for ubiquitination. Molecular Pharmacology 64: 334–345.

32. Luo X, Budihardjo I, Zou H, Slaughter C, Wang X (1998) Bid, a Bcl2 interacting protein, mediates cytochrome c release from mitochondria in response to activation of cell surface death receptors. Cell 94: 481–490.

33. Kim H, Rafiuddin-Shah M, Tu H-C, Jeffers JR, Zambetti GP, et al. (2006) Hierarchical regulation of mitochondrion-dependent apoptosis by BCL-2 subfamilies. Nature Cell Biology 8: 1348–1358.

34. Du C, Fang M, Li Y, Li L, Wang X (2000) Smac, a mitochondrial protein that promotes cytochrome c-dependent caspase activation by eliminating IAP inhibition. Cell 102: 33–42.

35. Maler O, Nickovic D (2004) Monitoring Temporal Properties of Continuous Signals. Proceedings of Formal Techniques, Modelling and Analysis in Real-Time and Fault-Tolerant Systems Conference. Springer. pp. 152–166.

36. Donzé A, Fanchon E, Gattepaille LM, Maler O, Tracqui P (2011) Robustness analysis and behavior discrimination in enzymatic reaction networks. PloS One 6: e24246.

37. Rehm M, Dussmann H, Janicke RU, Tavare JM, Kogel D, et al. (2002) Single-cell fluorescence resonance energy transfer analysis demonstrates that caspase activation during apoptosis is a rapid process. Role of caspase-3. The Journal of Biological Chemistry 277: 24506–24514.

38. Barnat J, Brim L, Cerna I, Drasan S, Safranek D (2008) Parallel Model Checking Large-Scale Genetic Regulatory Networks with DiVinE. Electronic Notes in Theoretical Computer Science 194: 35–50.

39. Batt G, Yordanov B, Weiss R, Belta C (2007) Robustness analysis and tuning of synthetic gene networks. Bioinformatics 23: 2415–2422.

40. Batt G, Page M, Cantone I, Goessler G, Monteiro P, et al. (2010) Efficient parameter search for qualitative models of regulatory networks using symbolic model checking. Bioinformatics 26: i603–10.

41. Bernot G, Comet J-P, Richard A, Guespin J (2004) Application of formal methods to biological regulatory networks: extending Thomas' asynchronous logical approach with temporal logic. Journal of Theoretical Biology 229: 339–347.

42. Donaldson R, Gilbert D (2008) A model checking approach to the parameter estimation of biochemical pathways. Computational Methods in Systems Biology: 269–287.

43. Fisher J, Piterman N, Hajnal A, Henzinger T a (2007) Predictive modeling of signaling crosstalk during C. elegans vulval development. PLoS Computational Biology 3: e92.

44. Jha SK, Clarke EM, Langmead CJ (2009) A bayesian approach to model checking biological systems. Computational Methods in Systems Biology 5688: 218–234.

45. Heath J, Kwiatkowska M, Norman G, Parker D, Tymchyshyn O (2008) Probabilistic model checking of complex biological pathways. Theoretical Computer Science 391: 239–257.

46. Donzé A, Maler O (2010) Robust satisfaction of temporal logic over real-valued signals. Formal Modeling and Analysis of Timed Systems: 92–106.

47. Albeck JG, Burke JM, Aldridge BB, Zhang M, Lauffenburger DA, et al. (2008) Quantitative analysis of pathways controlling extrinsic apoptosis in single cells. Molecular Cell 30: 11–25.

48. Agard NJ, Mahrus S, Trinidad JC, Lynn A, Burlingame AL, et al. (2012) Global kinetic analysis of proteolysis via quantitative targeted proteomics. Proceedings of the National Academy of Sciences of the United States of America 109: 1913–1918.

49. Maas C, Verbrugge I, de Vries E, Savich G, van de Kooij LW, et al. (2010) Smac/DIABLO release from mitochondria and XIAP inhibition are essential to limit clonogenicity of Type I tumor cells after TRAIL receptor stimulation. Cell Death and Differentiation 17: 1613–1623.

50. Avriel M (2003) Nonlinear programming: analysis and methods. Courier Dover Publications.

51. Hansen N, Ostermeier A (2001) Completely derandomized self-adaptation in evolution strategies. Evolutionary Computation 9: 159–195.

52. Kober a MM, Legewie S, Pforr C, Fricker N, Eils R, et al. (2011) Caspase-8 activity has an essential role in CD95/Fas-mediated MAPK activation. Cell Death and Disease 2: e212.

53. Fainekos GE, Pappas GJ (2009) Robustness of temporal logic specifications for continuous-time signals. Theoretical Computer Science 410: 4262–4291.

54. Rizk A, Batt G, Fages F, Soliman S (2011) Continuous valuations of temporal logic specifications with applications to parameter optimization and robustness measures. Theoretical Computer Science 412: 2827–2839.

55. Klipp E, Herwig R, Kowald A, Wierling C, Lehrach H (2005) Systems Biology in Practice. Concepts, Implementation and Application. Wiley-VCH.

56. Szallasi Z, Stelling J, Periwal V (2010) System Modeling in Cellular Biology: From Concepts to Nuts and Bolts. MIT Press.

57. Ghosh S, Matsuoka Y, Asai Y, Hsin K-Y, Kitano H (2011) Software for systems biology: from tools to integrated platforms. Nature Reviews Genetics 12: 821–832.

58. Serban R, Hindmarsh A (2005) CVODES, the sensitivity-enabled ODE solver in SUNDIALS. Proceedings of IDETC/CIE 2005.

Supplementary Information

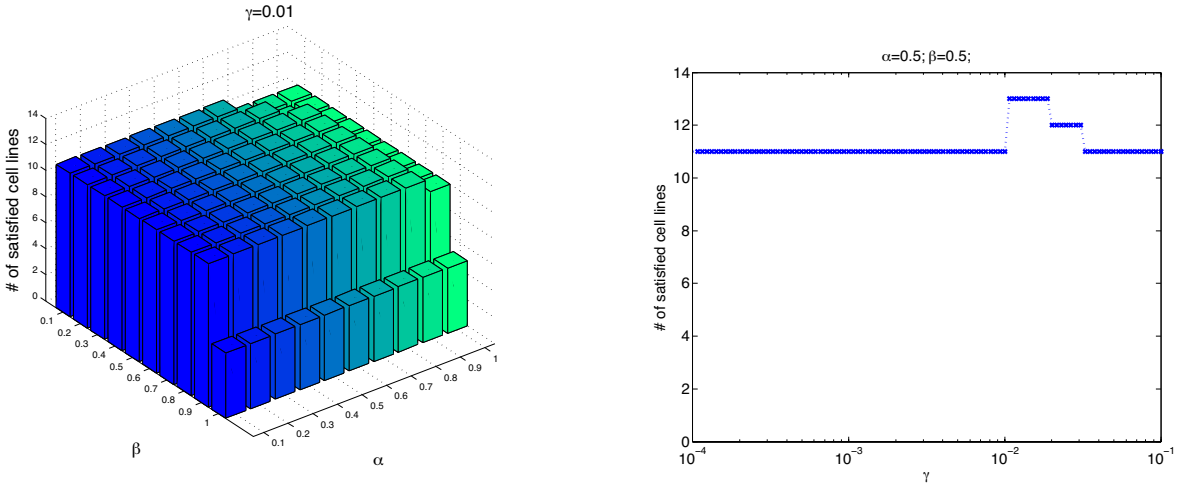

(A) (B)

Figure S1. Formula robustness. Number of matches between predicted and observed satisfaction values of the Properties 1-3 in all HCT116 and SKW6.4 cell lines (see Table 1). Full consistency with all experimental data corresponds to 16 matches (15 in the Table 1 and, additionally, p2(SKW6.4)= True). For original parameter values, independent from the choice of threshold values, we found at least three mismatches (see Table 1 in the main text). This number is robust with respect to changes of the PARP-related threshold, α, defining the *alive* property, and of the Apaf-related threshold, β, defining the *MOMP* occurance (see formulas below). It is also robust to the caspase activation threshold, γ, provided that this value remains low enough (i.e. <2%). Formulas: *p1:= always*$_{[0\text{-}6h]}$*(cPARP/PARP*$_{total}$< α); *Property2:= eventually(Casp8*$_{active}$ *and always*$_{[0\text{-}1h]}$ *not Casp3*$_{active}$*) where Casp8*$_{active}$*:= Casp8*/Casp8*$_{total}$> γ*, and Casp3*$_{active}$*:= Casp3*/Casp3*$_{total}$> γ*; p3:= Apaf*$_{free}$*/Apaf*$_{total}$< β *release (cPARP/PARP*$_{total}$<α*))*

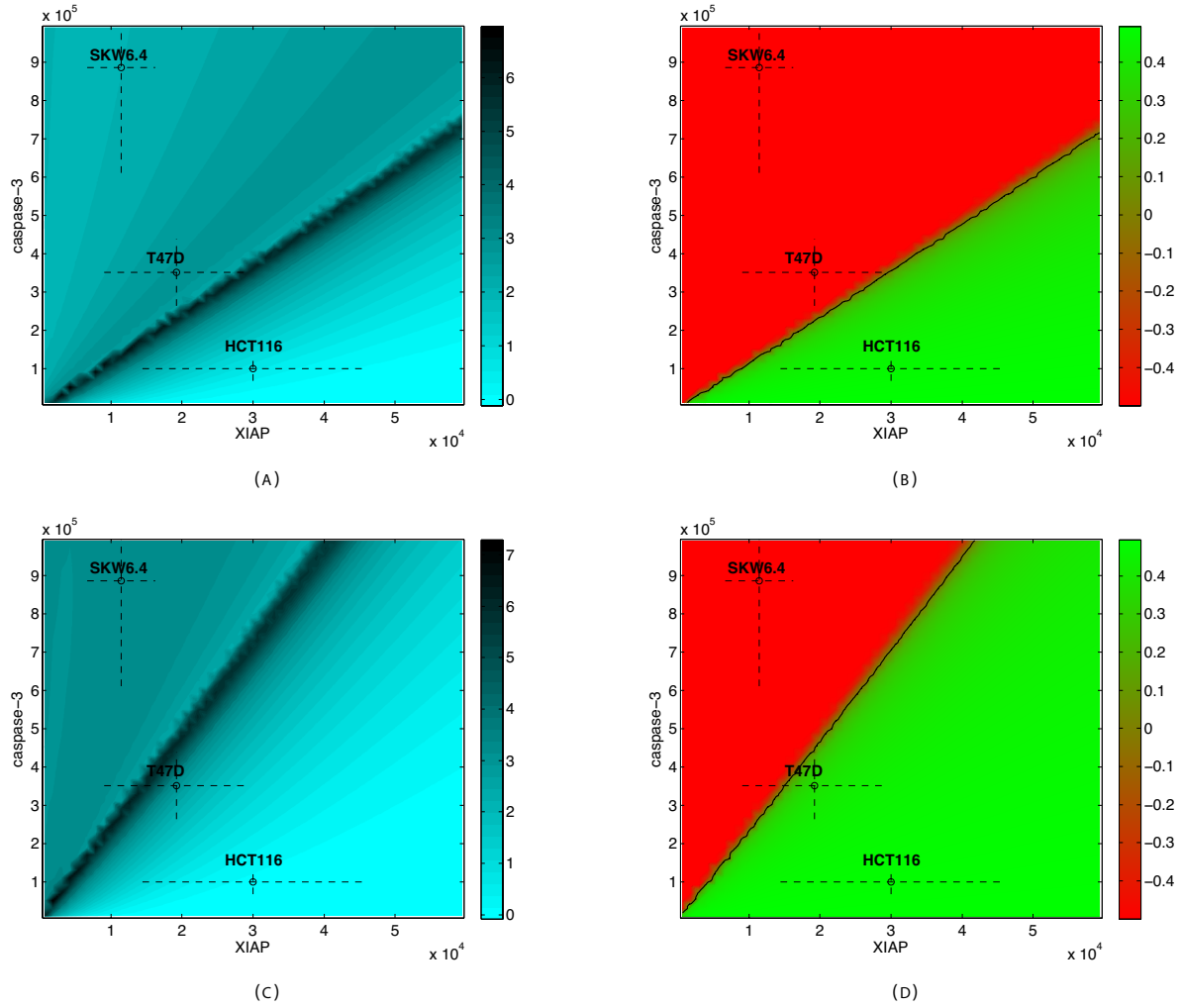

Figure S2. Comparison between DLE and Property 1 STL diagrams. Diagrams representing the values of the DLE computed at time T (A,C) and of the STL Property:= $always_{[0\text{-}T]}(\ cPARP/PARP_{total} < 0.5)$ (B,D) for T=6h (A-B) and T=4h (C-D). Strikingly, the separatrix is exactly at the same position, suggesting that DLE and Property 1 capture the same behavior. One should note that the interpretation of low DLE values is ambiguous, since low values are found in regions corresponding to type I (SKW6.4) and to type II cell types (HCT116).

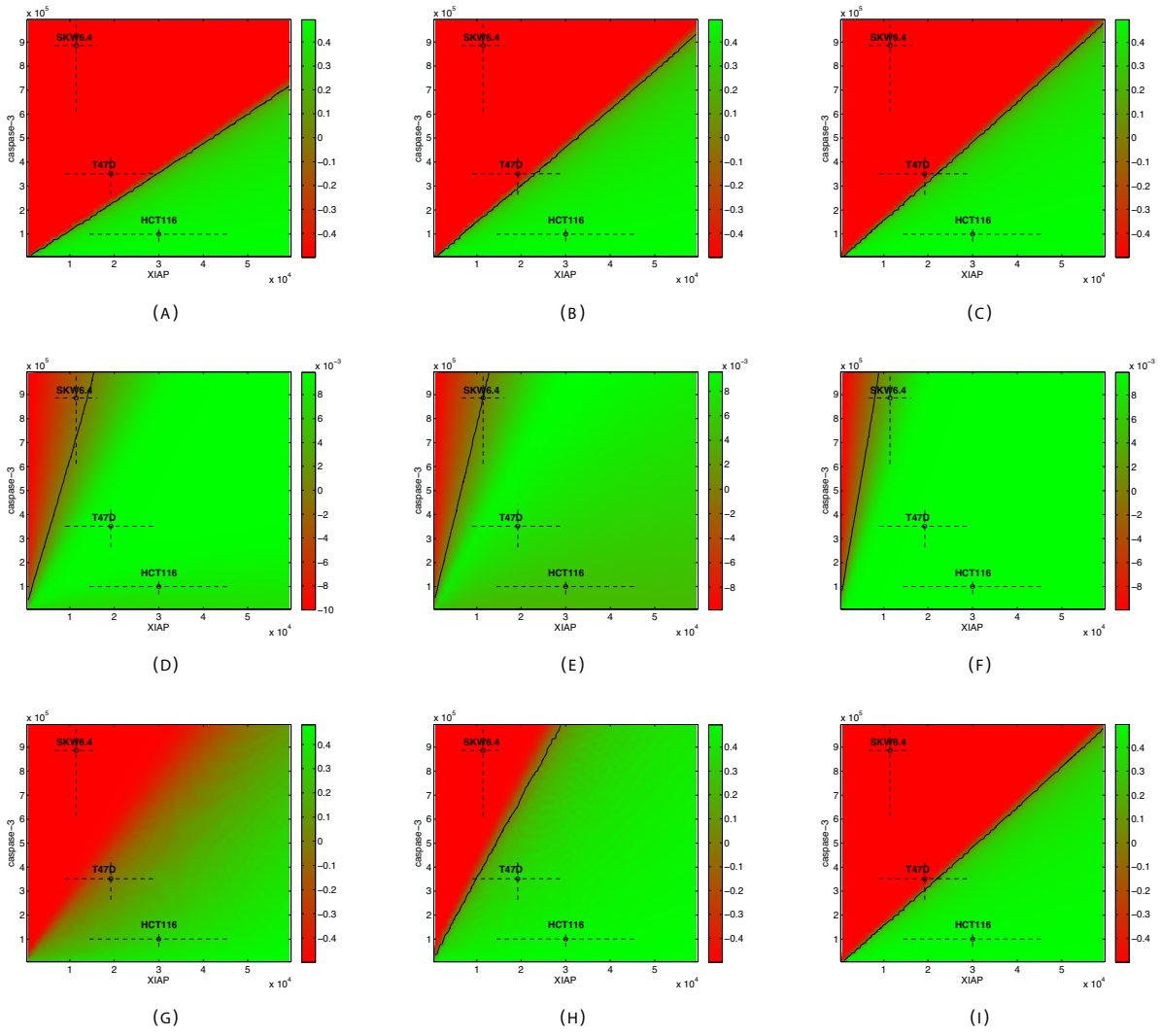

Figure S3. XIAP/Capsase-3 STL diagrams for all properties and HCT116, SKW6.4 and T47D measured protein concentrations. Diagrams representing the values of the STL properties p1, p2 and p3 (rows from top to bottom) using HCT116, SKW6.4, and T47D (columns from left to right) as nominal cells. Bcl2 is overexpressed in Property 1 diagrams (i.e. value for Bcl2 is 10 times higher than in the nominal cell in Table 2).In most cases, for a given property the satisfaction values associated with each cell type is similar irrespectively of the reference cell line used to construct the diagram. However, there are exceptions, like in the case of T47D cell line behavior (H and I). So care must be taken when interpreting STL diagrams. The same situation holds with DLE diagrams (not shown).

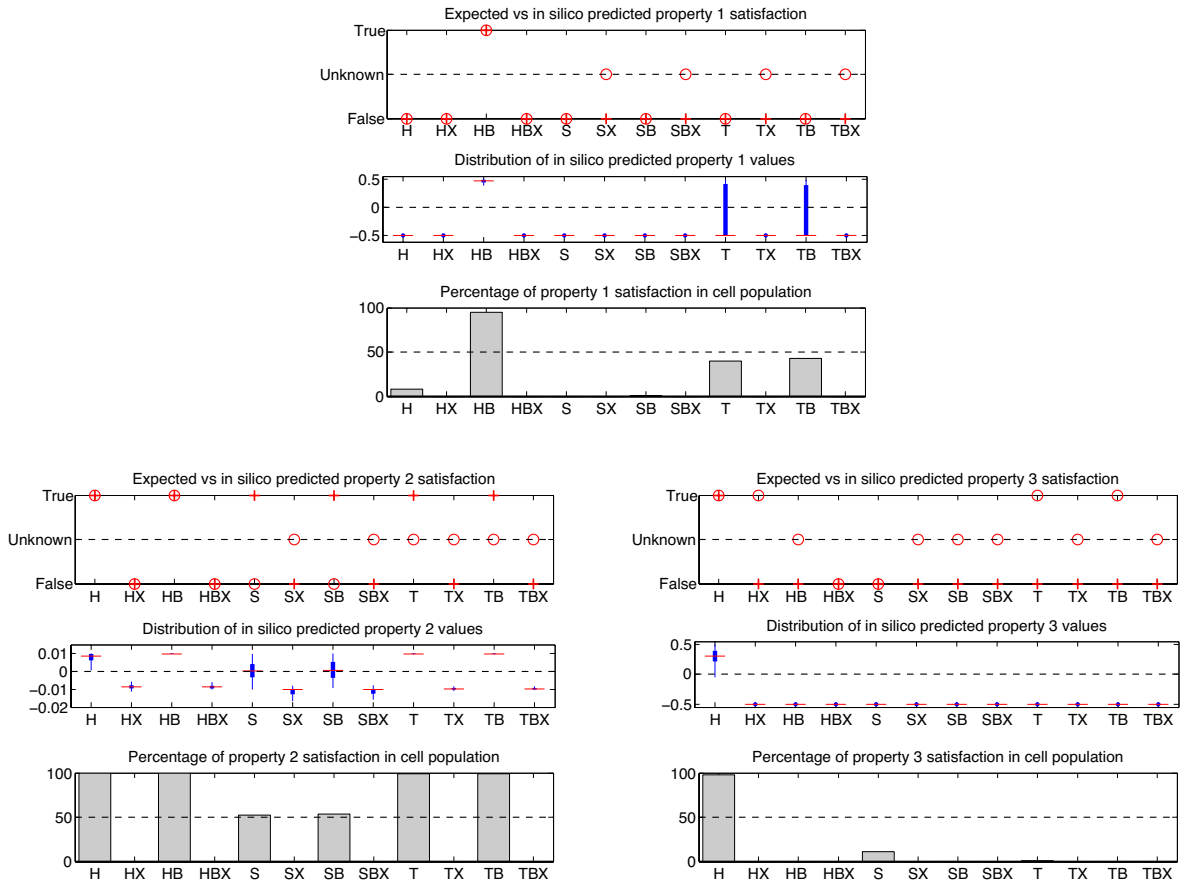

Figure S4. STL property values across all cell lines for Properties 1-3 for the EARM1.4. For each property plots indicate the nominal cell value (top), the distribution (middle), and the percentage of satisfaction (bottom) of the Property values for populations of cells of different cell lines. For distributions, box boundaries and red line indicate first and third quartiles, and median, respectively. When experimental data is available, circles in the True or False position in the top plot represent the expected values. These statistics are computed for populations of 5000 cells. The following abbreviations are used: H is HCT116, HX is ΔXIAP HCT116, HB is OE-Bcl2 HCT116, HBX is OE-Bcl2/ΔXIAP HCT116, S is SKW6.4, SX is ΔXIAP SKW6.4, SB is OE-Bcl2 SKW6.4, SBX is OE-Bcl2/ΔXIAP SKW6.4, T is T47D, TX is ΔXIAP T47D, TB is OE-Bcl2 T47D and TBX is OE-Bcl2/ΔXIAP T47D.

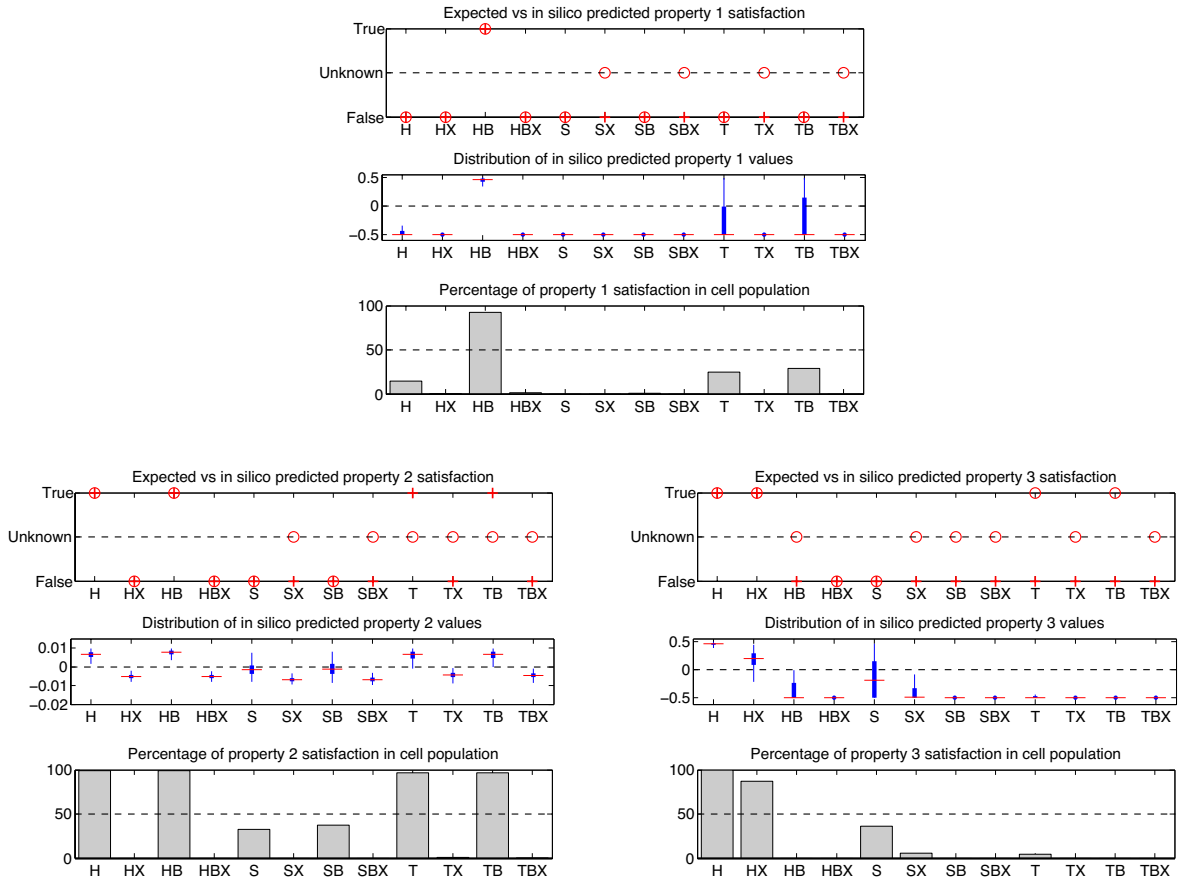

Figure S4. STL property values across all cell lines for Properties 1-3 for the EARM1.4 with corrected parameters from STable 1. For each property plots indicate the nominal cell value (top), the distribution (middle), and the percentage of satisfaction (bottom) of the Property values for populations of cells of different cell lines. For distributions, box boundaries and red line indicate first and third quartiles, and median, respectively. When experimental data is available, circles in the True or False position in the top plot represent the expected values. These statistics are computed for populations of 5000 cells. The following abbreviations are used: H is HCT116, HX is ΔXIAP HCT116, HB is OE-Bcl2 HCT116, HBX is OE-Bcl2/ΔXIAP HCT116, S is SKW6.4, SX is ΔXIAP SKW6.4, SB is OE-Bcl2 SKW6.4, SBX is OE-Bcl2/ΔXIAP SKW6.4, T is T47D, TX is ΔXIAP T47D, TB is OE-Bcl2 T47D and TBX is OE-Bcl2/ΔXIAP T47D.

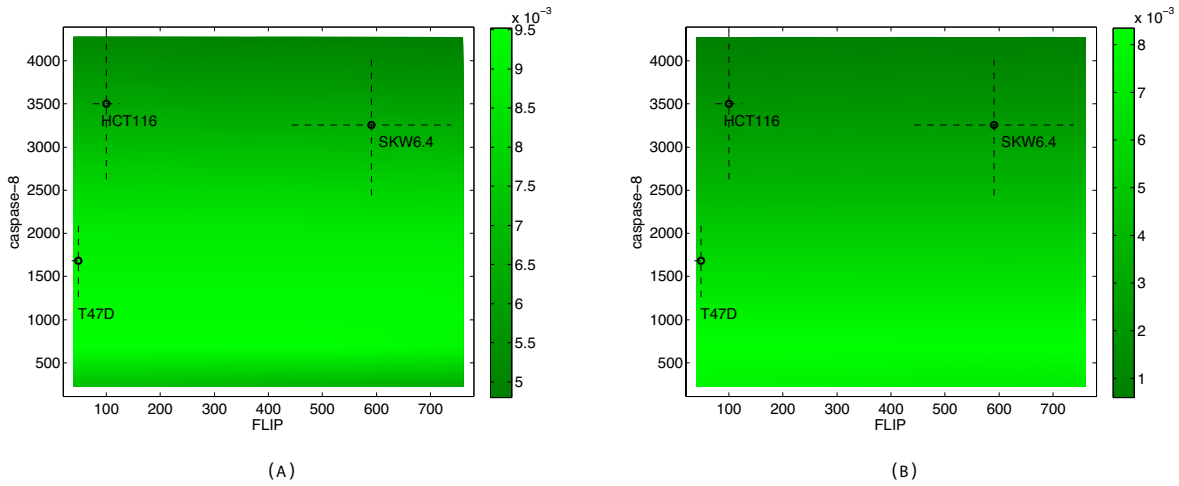

Figure S6. Property-2 phase diagrams for cells with inactivated caspase feedback loop. (A) Diagram computed with respect to ΔFB HCT116 cells. (B) Diagram computed with respect to ΔFB SKW6.4 cells. The removal of the feedback loop converts the SKW6.4 cells into a "type II cell" with respect to Property 2 (compare with Figure S7A).

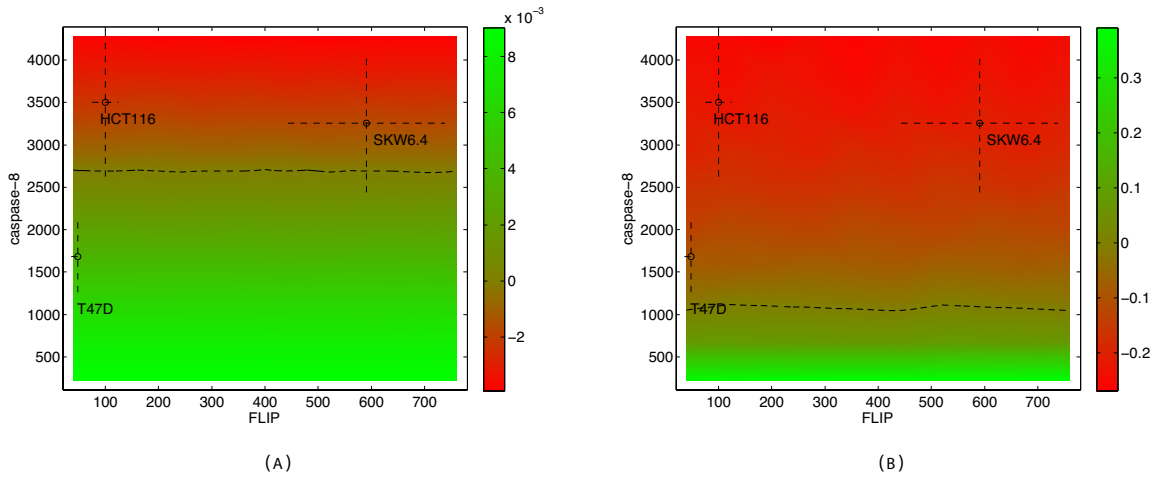

Figure S7. Phase diagrams for Property 2 (A) and Property 3 (B) in SKW6.4 cells. SKW6.4 cell exhibit type II behavior with respect to Property 2 and 3 even when the original or HC116 initial conditions are used. However, according to EARM1.4 low caspase-8 levels are able to change this behavior. According to the model it is possible to tune the level of caspase-8 such as Property 2 will be modified and Property 3 will remain unchanged.

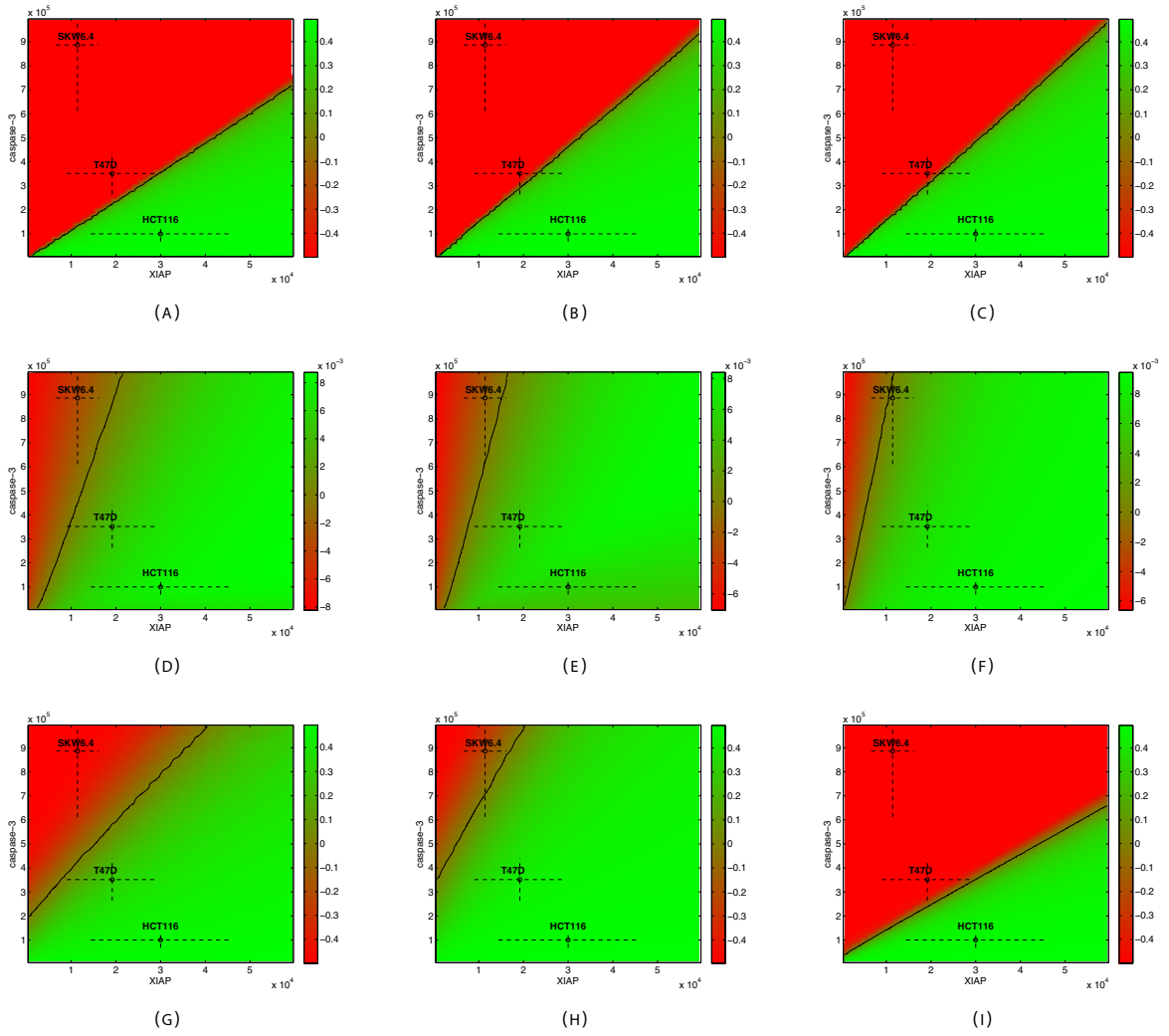

Figure S8. XIAP/Capsase-3 STL diagrams for all properties and HCT116, SKW6.4 and T47D measured protein concentrations computed using corrected EARM1.4 according to Table S1. Diagrams representing the values of the STL properties p1, p2 and p3 (rows from top to bottom) using HCT116, SKW6.4, and T47D (columns from left to right) as nominal cells. Bcl2 is overexpressed in Property 1 diagrams (i.e. value for Bcl2 is 10 times higher than in the nominal cell in Table 2).

	k7	kc9
New value	8.14e-8	1.80e-2
Original value	3.00e-8	1
Fold change	2.71	55.6

Table S1: Valid parameters. List of minimal parameter set leading to Property1-3 satisfaction for all but T47D cells, together with their new and original values, and the corresponding fold change.

RESEARCH CENTRE
ROCQUENCOURT

Domaine de Voluceau
Rocquencourt BP 105
78153 Le Chesnay Cedex France

Publisher
Inria
Domaine de Voluceau - Rocquencourt
BP 105 - 78153 Le Chesnay Cedex
inria.fr
ISSN 0249-6399